PREDICTING GENERATOR COUPLING USING POWER SYSTEM IMPEDANCE MATRICES

Except where reference is made to the work of others, the work described in this thesis is my own or was done in collaboration with my advisory committee. This thesis does not include proprietary or classified information.

_____
Kent Alexander Sayler

Certificate of Approval:

_____   _____
Charles A. Gross   S. Mark Halpin, Chair
Professor   Alabama Power Distinguished Professor
Electrical and Computer Engineering   Electrical and Computer Engineering

_____   _____
R. Mark Nelms   Stephen L. McFarland
Professor   Dean
Electrical and Computer Engineering   Graduate School

PREDICTING GENERATOR COUPLING USING POWER SYSTEM IMPEDANCE
MATRICES

Kent Alexander Sayler

A Thesis

Submitted to

the Graduate Faculty of

Auburn University

in Partial Fulfillment of the

Requirements for the

Degree of

Master of Science

Auburn, Alabama
May 11, 2006

PREDICTING GENERATOR COUPLING USING POWER SYSTEM IMPEDANCE
MATRICES

Kent Alexander Sayler

_____
Signature of Author

_____
Date of Graduation

VITA

Kent A. Sayler, son of Greg and Dianne Sayler, was born June 26, 1980 in York, Alabama. He graduated from Flomaton High School in 1998. For the next two years he attended Jefferson Davis Community College and he received his Associate of Science in May of 2000. He transferred to Auburn University in the Fall of 2000 where he enrolled in the College of Engineering. In December of 2003 he received his Bachelor of Electrical Engineering from Auburn University. He continued his education by becoming a graduate student in the Department of Electrical and Computer Engineering at Auburn University, where his research effort has been power system stability.

THESIS ABSTRACT

PREDICTING GENERATOR COUPLING USING POWER SYSTEM IMPEDANCE

MATRICES

Kent Alexander Sayler

Master of Science, May 11, 2006
(B.E.E., Auburn University, 2003)

69 Typed Pages

Directed by S. Mark Halpin

The combination of power flows on multiple lines constitutes a flowgate.

Transmission flowgates are one tool being used to deal with wide-area stability issues

because experience with dynamic simulation suggests that proximity to a stability limit

may be approximated using a transmission flowgate. An inconvenience associated with

flowgates, however, is the absence of a defined procedure by which to identify where

they need to be implemented in the power system. Knowing which machines swing

together as a result of a disturbance somewhere in the system is helpful when considering

possible flowgate locations. The concept of how the system impedance matrix can be

used to determine which generators in the power system move together for a given

contingency is discussed in this thesis.

Once a mathematical model of a multi-machine power system is formed, the system impedance matrix can be extracted from this model and used to suggest groups of machines which are likely to be electrically coupled together when the system is perturbed. The term "influence" will be used to refer to the degree to which impedances affect the total dynamic coupling because several factors affect the coupling between machines under dynamic conditions. This electrical coupling is validated by the in-phase behavior of generator rotor angles in the system. The generator rotor angle plots are obtained through time domain simulations and compared via visual inspection to the groups of machines as identified by the system impedance matrix values.

ACKNOWLEDGMENTS

I would like to express my sincere gratitude to all those people who provided a constant source of help and motivation throughout my work. First of all, I would like to thank my major professor and advisor Dr. S. Mark Halpin. I will always revere his patience, expert guidance and ability to solve intricate problems. He made my pursuit of higher education a truly enjoyable and unforgettable experience. I would also like to thank my committee members, Dr. Charles A. Gross and Dr. R. Mark Nelms for their help and valuable time they spent in reviewing this work. Last but certainly not least, I want to thank my wife, Marisa. She continually inspires me and is the sole reason I pursued a graduate degree.

Style manual of journal used <u>Graduate School: Guide to preparation and submission of theses and dissertations</u>

Computer software used <u>Microsoft Office 2003, MATLAB 6.5, Microsoft Visual Studio .NET 2003, PSS/E 28.0</u>

TABLE OF CONTENTS

LIST OF TABLES

LIST OF FIGURES

CHAPTER 1

INTRODUCTION

The continual increase of generation in localized areas is resulting in congested transmission lines within the power system. One kind of situation resulting from this congestion is the potential to threaten a system stability limit. One method used to help curtail congestion on transmission lines is the implementation of transmission flowgates. The idea of a transmission flowgate was originally constructed to deal with loop flows in interconnected systems and to manage overall power transfers from one control area to another. Experience with dynamic simulations suggests that proximity to a stability limit may be approximately predicted using a transmission flowgate [1].

The single-machine infinite bus (SMIB) system can be used to illustrate the usefulness of a flowgate, and it is shown in Figure 1.1.
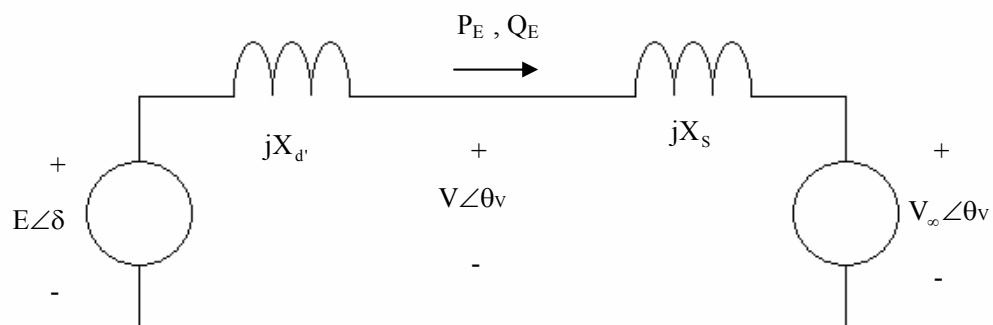
Figure 1.1 SMIB Positive Sequence Model

The terminal complex power can be expressed as a function of terminal voltage, machine internal voltage, machine reactance and system reactance as shown in (1.1).

$$\overline{S} = \frac{VE\sin(\delta - \theta_V)}{X_{d'}} + j\frac{VE\cos(\delta - \theta_V) - V^2}{X_{d'}} \tag{1.1}$$

It is important to recognize the assumptions associated with the SMIB system:

1. The machine under study is not large enough to influence the frequency of the bulk system. Therefore, the phase angle of the equivalent system is constant and chosen to be the reference angle, 0°.

2. The machine under study is not large enough to influence the voltage of the bulk system. Therefore, the voltage magnitude of the equivalent system is constant.

The amount of real and reactive power that will move from the generator to the system is represented by the first and second terms of (1.1), respectively. The real part of (1.1) is rewritten in (1.2). Notice in (1.2) that θ_V is no longer present because it is chosen as the reference angle.

$$P_E = \frac{VE}{X}\sin(\delta) \tag{1.2}$$

Observation of (1.2) reveals that there is a maximum amount of real power that can be moved from the machine under study to the rest of the system. This maximum amount of real power is obtained when the rotor angle, δ, reaches 90°. The rotor angle and speed of the machine are determined by the classical swing equation that relates the machine shaft angle with applied power as shown in (1.3).

$$\frac{d\omega}{dt} = \frac{\pi f}{H}\{P_M - P_E\}$$
$$\frac{d\delta}{dt} = \omega$$

(1.3)

In (1.3):

H is the inertia constant in seconds;

f is the nominal frequency in Hertz and is constant (not affected by changes in ω);

P_M is the mechanical power input for the machine and is assumed constant;

P_E is the electrical power output for the machine; and

ω is the relative angular velocity (with respect to a synchronous reference) of the rotor of the machine.

For the SMIB case, the worst-case stability scenario is when the electrical power, P_E, drops to zero during a fault [2]. For this situation, the swing equation in (1.3) reduces to that shown in (1.4) by using a double integration with respect to time.

$$\delta(t) = \frac{\pi f}{2H} P_M t^2 + \delta_0$$

(1.4)

Substituting δ_{cc} for $\delta(t)$ and solving for t produces (1.5), where t_{cc} represents the maximum time available to clear the worst-case fault, or the critical clearing time.

$$t_{cc} = \sqrt{(\delta_{cc} - \delta_0)\left(\frac{2H}{\pi f P_M}\right)}$$

(1.5)

In (1.5), the angles δ_{cc} and δ_0 represent the clearing time dependence on pre-contingency and post-contingency electrical system conditions, and P_M represents the pre-contingency mechanical power input to the generator, which is very nearly equal to P_E. It is clear from (1.5) that the critical clearing time is inversely proportional to the square root of P_M. In cases of practical interest, the critical clearing time t_{cc} is fixed by

3

circuit breaker and relay operating times. For a generation owner, the power output (and input P_M) is varied to meet economic goals. Therefore, it is a simple matter to solve (1.5) for the maximum permissible power output (and input, $P_{M,max}$) such that generator stability is maintained for a given t_{cc}[1]. Because P_M is approximately equal to P_E, it is possible to monitor the power flow on the branch from the machine under study to the system and accurately predict P_M. For the SMIB system shown in Figure 1.1, this single measurement of P_M constitutes the most basic flowgate because it is limiting only one element. The resulting equation for the SMIB flowgate is shown in (1.6).

$$P_M \leq P_{M,max} \tag{1.6}$$

The case where a single machine is connected to the power system through multiple lines is shown in Figure 1.2. As with the SMIB example, only one machine is limited. This means the flowgate completely surrounds the machine under study, G_1. For the case where G_1 is connected by multiple branches, (1.6) is slightly modified to account for both lines connected to bus 1 and is shown in (1.7).

$$P_M = P_{12} + P_{13} \leq P_{M,max} \tag{1.7}$$
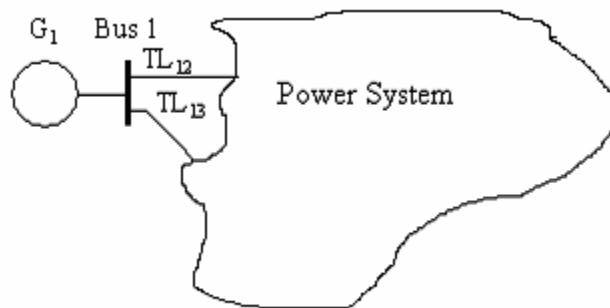
Figure 1.2 Single Machine with Multiple Lines

For a multi-machine case, it also is possible to monitor the power flow on multiple transmission lines and accurately predict P_M, because P_M is approximately equal to the electrical power injected into the network. The combination of power flows on multiple lines constitutes the flowgate; assuming there is a negligible amount of load inside the flowgate, this flowgate total is an accurate representation of P_M and can therefore be compared to $P_{M,max}$ to assess generator stability[1].

One problem with flowgates, however, is that no real procedure to define and place one in the system exists. One possible way to help identify potential flowgate locations would be to determine which generators in the system will "swing together" when the system is perturbed. The concept of how the system impedance matrix can be used to determine which generators in the power system move together for a given contingency is discussed in this thesis.

The first step of building a mathematical model of the power system is discussed in Chapter 2. The mathematical model will be a set of nonlinear coupled differential equations and includes models for system generators, loads, and the transmission network. After developing the model, a relationship for the electrical power output for a machine in the system in terms of all known quantities except machine rotor angles can be formed.

Once the system is modeled, a relationship between system impedance and generator coupling will be formed in Chapter 3 from examining the power system model equations. This generator coupling will then be verified by performing dynamic simulations on a 5-bus power system and comparing machine rotor angle plots to the coupling relationships specified by the system impedance matrix.

In Chapter 4, the generator coupling method will be further tested by introducing the Western States Coordinating Council (WSCC) 179-bus test system. The methods introduced in Chapter 3 will be applied to the larger 179-bus system for two cases: when a disturbance is close to a particular group of machines and when a disturbance is far away from the same group of machines.

A group of strongly coupled machines represent a stability concern because if any machine within the group goes unstable, the strong coupling between it and the other machines in the group will most likely result in multiple machines going unstable. Therefore, generation within this coupled group most likely needs to be curtailed. The amount by which generation needs to be curtailed can be correlated to some $P_{M,max}$ that is equal to the flow on the flowgate which surrounds the group of strongly coupled machines. The system impedance matrix is one factor of the total coupling that exists between generators and observation of the equations to be developed will show that it is a significant one.

CHAPTER 2

MULTI-MACHINE STABILITY

A mathematical model of the power system must be constructed if stability studies are to be done. This involves determining models for system generators, loads, and the transmission network. After developing the model, a relationship for the electrical power output for a machine in the system in terms of all known quantities except machine rotor angles can be formed.

2.1 Plant and Machine Models

The generator model depicted in Figure 2.1 [3] is a positive sequence "voltage behind a reactance" model of a synchronous machine. This model is used to study the stability of a power system for a period of time of one second or less because during this period the system dynamic response is dependent largely on stored kinetic energy in rotating masses [2]. Studies can be conducted in a relatively short time because the classical model is the simplest model used in studies of power system dynamics and requires a minimum amount of data.

The reactance X_d' is the direct axis transient reactance and is used when the machine has just experienced a transient but has not yet reached steady state. This value is applicable from a time period of about three 60 Hz cycles to 1 second after a disturbance has occurred. The machine internal voltage magnitude, E, is controlled by
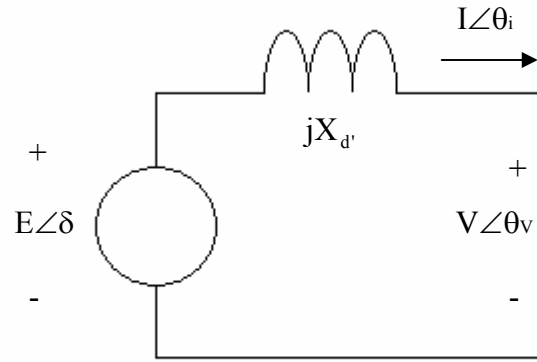
Figure 2.1 Positive Sequence Generator Model: Thevenin Form

the machine rotor speed and the field excitation. It is considered constant due to the facts

that speed changes are minimal and exciter response is limited during the first second

after a disturbance. The internal rotor angle, δ, depends on the angle between the stator

and rotor magnetic fields of a synchronous machine [2].

When the power system is extended to a multi-machine case, the model shown in

Figure 2.1 along with the assumptions discussed previously still applies, recognizing that

several of these models will be included. It is convenient to convert (via source
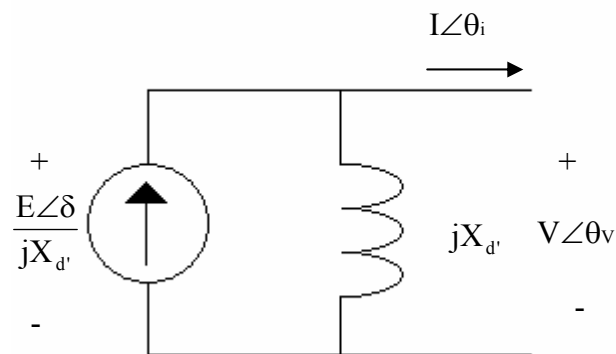
Figure 2.2 Positive Sequence Generator Model: Norton Form

transformation) the Thevenin model in Figure 2.1 into the Norton model shown in Figure 2.2.

2.2 Power System Model

The power system transmission network will be modeled as an admittance matrix. Consider the n-bus power system with each node specifically identified as shown in Figure 2.3.

An admittance matrix model of the bulk power transmission system can be formed that mathematically relates the nodal current injections and voltages as shown in (2.1). The current and voltage vectors are of dimension (nx1) and the admittance matrix is of dimension (nxn).

$$\tilde{I} = [\overline{Y}]\tilde{V} \tag{2.1}$$

The admittance matrix, $[\overline{Y}]$, can be built as follows:

1. The diagonal entries, $\overline{Y}_{ii}$, are the sum of all admittances connected to node i.

2. The off-diagonal entries, $\overline{Y}_{ij}$, are the sum of the negative of admittances between node i and node j.

$$
\begin{bmatrix}
\overline{I}_1 \\
\vdots \\
\overline{I}_i \\
\overline{I}_j \\
\vdots \\
\overline{I}_n
\end{bmatrix}
=
\begin{bmatrix}
\overline{y}_{1,1} & \cdots & \overline{y}_{1,i} & \overline{y}_{1,j} & \cdots & \overline{y}_{1,n} \\
\vdots & \ddots & \cdots & \cdots & \cdot\cdot\cdot & \vdots \\
\overline{y}_{i,1} & \cdots & \overline{y}_{i,i} & \overline{y}_{i,j} & \cdots & \overline{y}_{i,n} \\
\overline{y}_{j,1} & \cdots & \overline{y}_{j,i} & \overline{y}_{j,j} & \cdots & \overline{y}_{j,n} \\
\vdots & \cdot\cdot\cdot & \vdots & \vdots & \ddots & \vdots \\
\overline{y}_{n,1} & \cdots & \overline{y}_{n,i} & \overline{y}_{n,j} & \cdots & \overline{y}_{n,n}
\end{bmatrix}
\begin{bmatrix}
\overline{V}_1 \\
\vdots \\
\overline{V}_i \\
\overline{V}_j \\
\vdots \\
\overline{V}_n
\end{bmatrix}
\tag{2.2}
$$
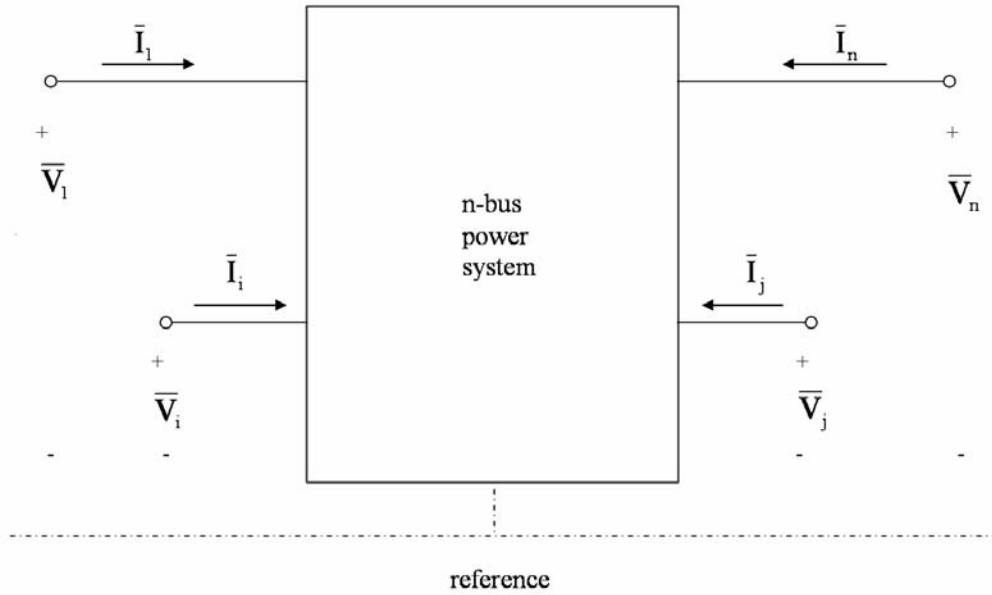
Figure 2.3 General Power System Model

2.3 The Complete Mathematical Model

To complete the model of the power system, the effects of machines and loads must be considered with the bulk transmission system in a single relationship. The effects of the machine are accounted for as follows:

1. The machine impedance, X_d', is converted to an admittance and included in the appropriate diagonal entry of the admittance matrix.

2.   The machine current is included in the current injection vector, $\tilde{I}$.

Loads are modeled as simple impedances at their respective buses. This can be done due to the fact that complex power and voltage is known for a given load. As a result, the equivalent shunt admittance of a load, $\overline{Y}_L$, can be calculated using (2.3).

$$\overline{Y}_L = \frac{P_L}{V_L{}^2} - j\frac{Q_L}{V_L{}^2}$$

(2.3)

10

2.4 Reducing the System Model

Careful evaluation of (2.2) reveals that for an n-bus power system, if i buses are machine buses, then n-i buses are non-machine buses. All the buses except for the generator buses can be eliminated, thus reducing the dimension of the admittance matrix. This reduction, known as Kron reduction, is performed by matrix operations considering the fact that all buses which do not contain a generator have a current injection that is equal to zero.

The first step is assigning machine buses the numbers 1 through m and all other buses (ones without machines) are numbered (1+m) through n. The revised version of (2.2) is shown in (2.4).

$$
\begin{bmatrix} \bar{I}_1 \\ \vdots \\ \bar{I}_m \\ \bar{I}_{m+1} \\ \vdots \\ \bar{I}_n \end{bmatrix} = \begin{bmatrix} \bar{y}_{1,1} & \cdots & \bar{y}_{1,m} & \bar{y}_{1,m+1} & \cdots & \bar{y}_{1,n} \\ \vdots & \ddots & \cdots & \cdots & \ddots & \vdots \\ \bar{y}_{m,1} & \cdots & \bar{y}_{m,m} & \bar{y}_{m,m+1} & \cdots & \bar{y}_{m,n} \\ \bar{y}_{m+1,1} & \cdots & \bar{y}_{m+1,m} & \bar{y}_{m+1,m+1} & \cdots & \bar{y}_{m+1,n} \\ \vdots & \ddots & \vdots & \vdots & \ddots & \vdots \\ \bar{y}_{n,1} & \cdots & \bar{y}_{n,m} & \bar{y}_{n,m+1} & \cdots & \bar{y}_{n,n} \end{bmatrix} \begin{bmatrix} \bar{V}_1 \\ \vdots \\ \bar{V}_m \\ \bar{V}_{m+1} \\ \vdots \\ \bar{V}_n \end{bmatrix}
\tag{2.4}
$$

Using the new subscripts denoted in (2.4), (2.5) is written and shown below, where the subscript 'G' is equal to m and the subscript 'S' is equal to (n-m).

$$
\begin{bmatrix} \tilde{I}_G \\ \tilde{I}_S \end{bmatrix} = \begin{bmatrix} [Y_{GG}] & [Y_{GS}] \\ [Y_{SG}] & [Y_{SS}] \end{bmatrix} \begin{bmatrix} \tilde{V}_G \\ \tilde{V}_S \end{bmatrix}
\tag{2.5}
$$

Recognizing that there are no current injections at buses that do not contain machines, the current vector, $\tilde{I}_S$, is equal to zero. Therefore, (2.5) can be expanded as shown in (2.6) and (2.7).

$$
\tilde{I}_G = [Y_{GG}]\tilde{V}_G + [Y_{GS}]\tilde{V}_S
\tag{2.6}
$$

11

$$\tilde{0} = [Y_{SG}]\tilde{\tilde{V}}_G + [Y_{SS}]\tilde{\tilde{V}}_S \tag{2.7}$$

Equation (2.7) can be solved for $\tilde{\tilde{V}}_S$ and the result can be substituted into (2.6) to obtain (2.8) and (2.9).

$$\tilde{\tilde{I}}_G = \left\{ [Y_{GG}] - [Y_{GS}][Y_{SS}]^{-1}[Y_{SG}] \right\} \tilde{\tilde{V}}_G \tag{2.8}$$

$$\tilde{\tilde{I}}_G = \left[\overline{Y}_G \right] \tilde{\tilde{V}}_G \tag{2.9}$$

Equation (2.9) is the admittance matrix model that includes the effects of system components but is a relationship strictly between generator current injections and generator terminal voltages.

2.5 The Multi-Machine Stability Problem

With all machines, power transmission equipment, and system loads included in (2.2), the entire model can be solved to determine all nodal voltages. The swing equation presented for the SMIB case in Chapter 1 is shown in (2.10) for a machine at bus i in the power system. All assumptions presented in Chapter 1 are still applicable for the multi-machine case.

$$\frac{d\omega_i}{dt} = \frac{\pi f}{H_i}\left\{ P_{M,i} - P_{E,i} \right\}$$
$$\frac{d\delta_i}{dt} = \omega_i \tag{2.10}$$

An expression can be developed for $P_{E,i}$ in terms of the power system component impedances and other machines using (2.9). The electrical power output based on Figure 2.3 for machine i is given in (2.11).

$$P_{E,i} = V_i I_i \cos(\theta_{v,i} - \theta_{i,i}) \tag{2.11}$$

12

Recognizing in (2.9) that each current injection is associated with a specific machine internal voltage and impedance allows (2.12) to be calculated for the ith machine.

$$\bar{I}_i = \frac{E_i \angle \delta_i}{jX'_{d,i}} \tag{2.12}$$

From (2.12), the current magnitude and angle in (2.11) are known for each machine. The terminal voltage, however, is unknown and must be expressed using (2.9). Assuming $[\bar{Y}]$ is non-singular and can therefore be inverted, (2.9) can be rewritten as (2.13), where $[\bar{Z}]$ is known as the impedance matrix.

$$\begin{bmatrix} \bar{V}_1 \\ \vdots \\ \bar{V}_i \\ \bar{V}_j \\ \vdots \\ \bar{V}_m \end{bmatrix} = \begin{bmatrix} \bar{z}_{1,1} & \cdots & \bar{z}_{1,i} & \bar{z}_{1,j} & \cdots & \bar{z}_{1,m} \\ \vdots & \ddots & \cdots & \cdots & \ddots & \vdots \\ \bar{z}_{i,1} & \cdots & \bar{z}_{i,i} & \bar{z}_{i,j} & \cdots & \bar{z}_{i,m} \\ \bar{z}_{j,1} & \cdots & \bar{z}_{j,i} & \bar{z}_{j,j} & \cdots & \bar{z}_{j,m} \\ \vdots & \ddots & \vdots & \vdots & \ddots & \vdots \\ \bar{z}_{m,1} & \cdots & \bar{z}_{m,i} & \bar{z}_{m,j} & \cdots & \bar{z}_{m,m} \end{bmatrix} \begin{bmatrix} \bar{I}_1 \\ \vdots \\ \bar{I}_i \\ \bar{I}_j \\ \vdots \\ \bar{I}_m \end{bmatrix} \tag{2.13}$$

Using (2.11)-(2.13), the machine electrical power output can be expressed as a summation involving all known quantities except machine rotor angles as shown in (2.14).

$$P_{E,i} = \frac{E_i}{X'_{d,i}} \sum_{j=1}^{m} \left\{ \frac{E_j}{X'_{d,j}} z_{ij} \cos\left(\delta_i - \delta_j - \zeta_{i,j}\right) \right\} \tag{2.14}$$

Substituting (2.14) into (2.10) yields (2.15), which is a complete set of equations of motion for machine i in terms of the power system component impedances and other machines.

$$\frac{d\omega_i}{dt} = \frac{\pi f}{H_i} \left\{ P_{M,i} - \frac{E_i}{X'_{d,i}} \sum_{j=1}^{m} \left\{ \frac{E_j}{X'_{d,j}} z_{ij} \cos\left(\delta_i - \delta_j - \zeta_{i,j}\right) \right\} \right\}$$

$$\frac{d\delta_i}{dt} = \omega_i$$

(2.15)

A relationship for the electrical power output for a machine has now been derived and is used to write the complete set of equations of motion in (2.15). The next step is to use the equations of motion in (2.15) to form a relationship between system impedance and generator coupling. Once developed, this relationship can be used to help identify potential flowgate locations within a power system.

CHAPTER 3

GENERATOR COUPLING AND THE POWER SYSTEM MODEL

A relationship between system impedance and generator coupling can be formed by examining the equation that models the electrical power output for a machine in the system in terms of all known quantities except machine rotor angles. This generator coupling can then be verified by performing dynamic simulations on a given power system and comparing machine rotor angle plots to the coupling relationships predicted by the system impedance matrix.

3.1 System Impedance and Electrical Power Output

The equations of electrical power output, bus voltage (in terms of impedance), and the swing equation developed in Chapter 2 are repeated in (3.1) – (3.3).

$$
\begin{bmatrix} \overline{V}_1 \\ \vdots \\ \overline{V}_i \\ \overline{V}_j \\ \vdots \\ \overline{V}_m \end{bmatrix} = \begin{bmatrix} \overline{z}_{1,1} & \cdots & \overline{z}_{1,i} & \overline{z}_{1,j} & \cdots & \overline{z}_{1,m} \\ \vdots & \ddots & \cdots & \cdots & \ddots & \vdots \\ \overline{z}_{i,1} & \cdots & \overline{z}_{i,i} & \overline{z}_{i,j} & \cdots & \overline{z}_{i,m} \\ \overline{z}_{j,1} & \cdots & \overline{z}_{j,i} & \overline{z}_{j,j} & \cdots & \overline{z}_{j,m} \\ \vdots & \ddots & \vdots & \vdots & \ddots & \vdots \\ \overline{z}_{m,1} & \cdots & \overline{z}_{m,i} & \overline{z}_{m,j} & \cdots & \overline{z}_{m,m} \end{bmatrix} \begin{bmatrix} \overline{I}_1 \\ \vdots \\ \overline{I}_i \\ \overline{I}_j \\ \vdots \\ \overline{I}_m \end{bmatrix} \tag{3.1}
$$

$$
P_{E,i} = \frac{E_i}{X'_{d,i}} \sum_{j=1}^{m} \left\{ \frac{E_j}{X'_{d,j}} z_{ij} \cos(\delta_i - \delta_j - \zeta_{i,j}) \right\} \tag{3.2}
$$

$$
\frac{d\omega_i}{dt} = \frac{\pi f}{H_i} \left\{ P_{M,i} - \frac{E_i}{X'_{d,i}} \sum_{j=1}^{m} \left\{ \frac{E_j}{X'_{d,j}} z_{ij} \cos(\delta_i - \delta_j - \zeta_{i,j}) \right\} \right\}
$$
$$
\frac{d\delta_i}{dt} = \omega_i \tag{3.3}
$$

15

Direct examination of (3.2) brings insight into how generation at a particular bus affects conditions at other buses. For instance, the influence of generator j on real power injected at bus i is quantified by $\dfrac{E_i}{X'_{d,i}}\left\{\dfrac{E_j}{X'_{d,j}}z_{ij}\right\}$. Also, the voltage at bus i due to the current injected at bus j is seen in the $\dfrac{E_j}{X'_{d,j}}z_{ij}$ term.

Further examination of (3.2) shows that there is a relationship between system impedance and the electrical power output of each machine in a given system. Consider a disturbance represented by a 1 per-unit current injection at bus i in the system. From (3.1), this injection at bus i (and only at bus i) will result in voltages being produced at all other buses j in the system based on the product $z_{ij}*I_i$. In (3.2), the current injection magnitude at bus i is represented by the $\dfrac{E_i}{X'_{d,i}}$ term and the bus voltage magnitude at bus i is represented by the $\displaystyle\sum_{j=1}^{n}\left\{\dfrac{E_j}{X'_{d,j}}z_{ij}\right\}$ term. Therefore, a voltage produced at bus i will have the effect of increasing the electrical power output from the machine at bus i.

Consider the effect on the terminal (i.e. bus) voltage i due to a current injection at bus j that is quantified by $\dfrac{E_j}{X'_{d,j}}z_{ij}$. As stated in Chapter 1, there is a maximum amount of real power that can be moved from a machine to the rest of the system. This maximum power is defined in (1.2) where V is the terminal voltage magnitude, E is the machine internal voltage magnitude, X is machine and system impedance, and δ is the machine rotor angle. The variables E and X are constant, which means anything that affects V will impact stability more significantly than something that has little affect on V. The z_{ij}

term in $\dfrac{E_j}{X'_{d,j}} z_{ij}$ is an indicator of how a current injection at bus j affects V at bus i and

therefore the response of the generator at bus i.

From (3.3), it can be seen that because the mechanical power input from machine j is constant, the equilibrium between the input and output power will be upset if electrical power output is increased. This loss of equilibrium causes the rotor angle of machine j to increase or decrease according to the laws of motion of a rotating body [2]. During a disturbance, two machines are said to be electrically coupled if their rotor angles swing in phase with each other.

For a current injection from a generator at bus i, one factor that could indicate if machines in a system will swing together (i.e. are strongly coupled) is the magnitude of the off-diagonal z_{ij} terms in the impedance matrix. This is due to the fact that a larger z_{ij} entry in the column corresponding to bus j will result in a larger change in rotor angle because of the direct relationship between angular velocity and impedance seen in (3.3). If machines at various buses are not strongly influenced by each other, then they may not swing together when disturbed. The extent to which a disturbance at bus i is felt at bus j is shown in $[\overline{Z}]$. The same principle applies to indicate the extent to which the behavior of a generator at bus i has on bus j. Because i and j both contain generators, $[\overline{Z}]$ can be considered to show at least part of the influence generator i has on generator j. Therefore, by looking at the magnitude of the z_{ij} terms in (3.1), some indication of how much impact a current injection at bus j has on all other buses i=1…m can be obtained.

Further observation of (3.2) reveals that X'_d can also have a similar influence on how the behavior of a generator at bus i can possibly affect bus j. This is because the

17

effects predicted by the magnitude of the z_{ij} terms in (3.1) are altered by X'_d in the current injection. Each current injection in the vector in (3.1) contains an X'_d that scales each row of the system impedance matrix by its corresponding machine impedance. Therefore, for power systems where large variations in X'_d exist, X'_d becomes very important when considering how a current injection from a generator at a bus can possibly affect other buses in the power system.

3.2 5-Bus System Example

The 5-bus system [1] in Figure 3.1 will be used to illustrate the generator influence concept introduced in Section 3.1. The corresponding system information is detailed in Tables 3.1 – 3.2.

The admittance matrix, $[\overline{Y}]$, can be formed from the information given in Tables 3.1 and 3.2 as described in Section 2.2. Because $[\overline{Y}]$ is non-singular, the system impedance matrix, $[\overline{Z}]$, can be formed by inverting $[\overline{Y}]$. Kron reduction is then performed on $[\overline{Z}]$, which reduces it to a 4x4 matrix. Because bus 2 is the only non-generator bus, it
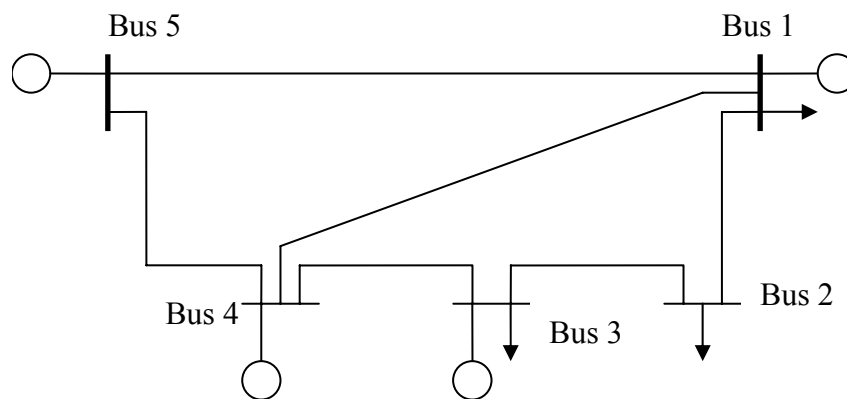

Figure 3.1 5-Bus Test System

18

Table 3.1 5-Bus System Bus and Machine Data

Bus #	V	δ	P_G	Q_G	P_L	Q_L
1	0.975	-15.98	110.0	53.2	350.0	87.7
2	0.978	-17.19	-	-	350.0	87.7
3	0.997	-15.61	160.0	251.8	350.0	87.7
4	1.0	-12.43	200.0	93.0	-	-
5*	0.995	-4.77	596.0	44.4	-	-

*Slack bus

Table 3.2 5-Bus System Branch Data

From	To	R	X	B	Rating
1	2	0.0014	0.0138	0.0284	502
1	4	0.0056	0.0552	0.1136	502
4	5	0.0042	0.0414	0.0858	502
2	3	0.0014	0.0138	0.0284	502
3	4	0.0014	0.0138	0.0284	502
1	5	0.0070	0.0690	0.142	502

Table 3.3 5-Bus Impedance Matrix Magnitudes, [Zij]

	1	5	3	4
1	0.0159	0.0033	0.0082	0.0072
5	0.0033	0.0094	0.0029	0.0037
3	0.0082	0.0029	0.015	0.0098
4	0.0072	0.0037	0.0098	0.0144

was simply swapped with bus 5 in the renumbering procedure. It is shown in Table 3.3,

however, by its original label of "5" so it will correspond with the bus labels seen in

Figure 3.1. The magnitudes of the resulting impedances are calculated and depicted in

tabular form in Table 3.3, where $z_{1,1}$=0.0159, $z_{1,5}$=0.0033, and so on.

As stated in Section 3.1, looking at the size of the z_{ij} terms in Table 3.3 will give

an indication of how much impact a current injection from a generator at a particular bus

will have at the other buses in the system. Inspection of the off-diagonals in Table 3.3

doesn't reveal much disparity in magnitude between the terms. For example, the

impedance magnitudes $z_{3,5}$ and $z_{4,5}$ differ by 0.0008 pu. The difference is even smaller

when other generator buses are compared. It appears that the behavior of a generator at a

particular bus will have similar effects on all generators in the 5-bus system, because all

relevant entries in the impedance matrix have magnitudes whose values are close in

proximity to each other.

Also, all machines in the 5-bus system have the same value for X'_d, which means

all the terms in $[\overline{Z}]$ are all effectively scaled by the same amount. The relative size of the

entries in $[\overline{Z}]$ to each other is an indicator of how generators can possibly influence one

another to a greater or lesser degree. If all entries in $[\overline{Z}]$ are scaled by the same amount,

X'_d has no overall effect on generator influence for the 5-bus system.

The impedance matrix entries will be different, however, if one or more branches

are taken out of service due to a contingency. It is this scenario where the size of the z_{ij}

terms will be quite informative.

A typical contingency that can create stability problems is a three-phase fault with

breaker failure [1]. Suppose that bus 4 is a straight bus with two bus sections connected

with a tiebreaker. The generator and TL_{45} are on one section, while the lines TL_{41} and

TL_{43} are on the other section. The contingency considered here is that a three-phase fault

occurs on TL_{43} and is just outside the substation of bus 4. For this breaker failure

contingency, let the bus 4 line breaker fail to clear. Assuming pilot relaying is present

and three cycle breakers are used, the bus 3 end of the faulted line clears in

approximately 4 cycles (66.67 ms for 60 Hz systems). Due to the stuck breaker, the

entire bus section is cleared in approximately 12 cycles (200 ms for 60 Hz systems) by

Table 3.4 5-Bus Impedance Matrix with Bus 4 Breaker Failure Contingency

	1	5	3	4
1	0.0195	0.0026	0.0115	0.0015
5	0.0026	0.0096	0.0015	0.0054
3	0.0115	0.0015	0.0232	0.0009
4	0.0015	0.0054	0.0009	0.0262

opening the tiebreaker and initiating a transfer trip operation to bus 1. Generator G_4

remains in service and connected to the system through TL_{45}.

The loss of TL_{41} and TL_{43} change the impedance matrix magnitudes as seen in

Table 3.4. Inspection of the off-diagonals with the two branches out of service yields a

much different result than before. The impedance magnitudes $z_{3,5}$ and $z_{4,5}$ differ by

0.0081 pu – a 1000% increase from the pre-fault system conditions. Observation of the

other columns of the impedance matrix also reveals larger magnitude disparities than in

the case with all lines in service. In the column corresponding to generator 1, the entries

corresponding to generators 4 and 5 both have a magnitude less than one-fifth the size of

the entry corresponding to generator 3. In the column corresponding to generator 3, the

entries corresponding to generators 4 and 5 both have a magnitude less than one-fifth of

the size of the entry corresponding to generator 1. The opposite effects are seen in the

columns corresponding to generators 4 and 5. In each case, the entries for generators 1

and 3 have much smaller magnitudes than the entry for the other generator in question.

As stated in Section 3.1, looking at the size of the z_{ij} terms in Table 3.4 can give

some indication of how much impact the behavior of a generator at a particular bus will

have on the other machines in the system. Because of the direct relationship between

impedance and angular velocity in (3.3), the largest off-diagonal magnitude in column j

of the system impedance matrix is indicative of the machine most affected by a current

injection from a machine at bus j. Observation of the current injection vector reveals that if a generator at bus j experiences a change in rotor angle, of the remaining generators in the system, the generator that will experience the greatest change in rotor angle corresponds to the largest off-diagonal entry in column j of the system impedance matrix. The larger that this magnitude is, the more influence that the generator at bus j has on this other generator. If the influence is large enough, the affected generator rotor angle can move in phase with the rotor angle of machine j. In this case of in-phase behavior, it can be said that these two machines could be strongly electrically coupled to each other.   In the 5-bus system example with two lines out of service, the large magnitudes of bus 4 in column 5 and bus 5 in column 4 indicate that the generator at bus 5 has a much stronger influence on the generator at bus 4 (and vice-versa) than on the generators at buses 1 and 3. Also, the large magnitudes of bus 3 in column 1 and bus 1 in column 3 indicate the generator at bus 1 has a much stronger influence on the generator at bus 3 (and vice-versa) than on the generators at buses 4 and 5.

Therefore, it would seem from observation of Table 3.4 that generators 4 and 5 strongly influence one another, while generators 1 and 3 also strongly influence each other. The presence of these two distinct groups can be verified by observing the frequency and phase characteristics of the machine rotor angle plots in Figure 3.2 which were obtained via dynamic simulation.

It is clear from observation of Figure 3.2 that if the generator at bus 5 experiences a large change in rotor angle, the generator at bus 4 will also experience this large change and possibly go unstable. The same can be said for generators 1 and 3. Reducing the output power of a generator increases the amount of time available to clear a worst-case
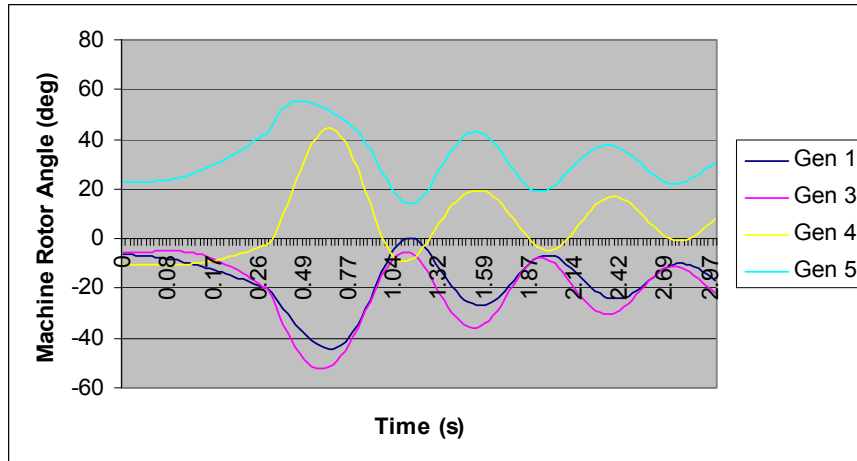
22

Figure 3.2 Rotor Angles for Breaker Failure Contingency at Bus 4

fault, according to the inverse relationship between power output and critical clearing time in (1.5). Therefore, the 5-bus system would be more likely to remain stable for the above contingency if the combined output power of generators 4 and 5 or 1 and 3 is held below some limiting value. One way this limiting value could be enforced is by defining a maximum amount of power allowed to flow on the lines that connect a group of generators to the rest of the power system. This means constraining the power flowing on lines TL_{51}, TL_{41}, and TL_{43}, and this constraint can be represented as a flowgate. The system impedance matrix concepts introduced in this chapter helped in identifying the two groups of coupled generators in the 5-bus system, as well as a possible flowgate location.

The relationship of generator coupling and system impedance appears to be valid at least for this particular 5-bus system. The next step is to consider a much larger power system to further verify the validity of this method.

CHAPTER 4

179-BUS SYSTEM EXAMPLE

In this chapter, the effect of system impedance on generator coupling is further

discussed by introducing the WSCC 179-bus test system. The methods introduced in

Chapter 3 will be applied to the larger 179-bus system for two cases: when a contingency

is close to a particular group of machines and when a contingency is far away from the

same group of machines.

4.1 WSCC 179-Bus Test System

The approach presented using the 5-bus system in Chapter 3 was applied to the

larger WSCC 179-bus system. The single line diagram for the 179-bus system is shown

in Figure 4.1. Closer looks at the four sub-sections of Figure 4.1 are shown in Figures

4.2 – 4.5. Figure 4.1 is necessary to give overall feel of the topography of the system

while the smaller maps are necessary for clarity of discussion of individual buses, lines,

and generators. The methods introduced in Chapter 3 will be used to identify possible

flowgate locations in the WSCC 179-bus system.

4.2 Graphical Depiction of Machine Coupling

For the 5-bus system introduced in Chapter 3, it was a trivial task to observe the

impedance matrix and determine how a current injection at one bus affected the other

buses in the system. This is due to the fact that the Kron-reduced $\left[\overline{Z}\right]$ for the 5-bus

system is only a 4x4 matrix. The WSCC 179-bus system presents a problem, however,
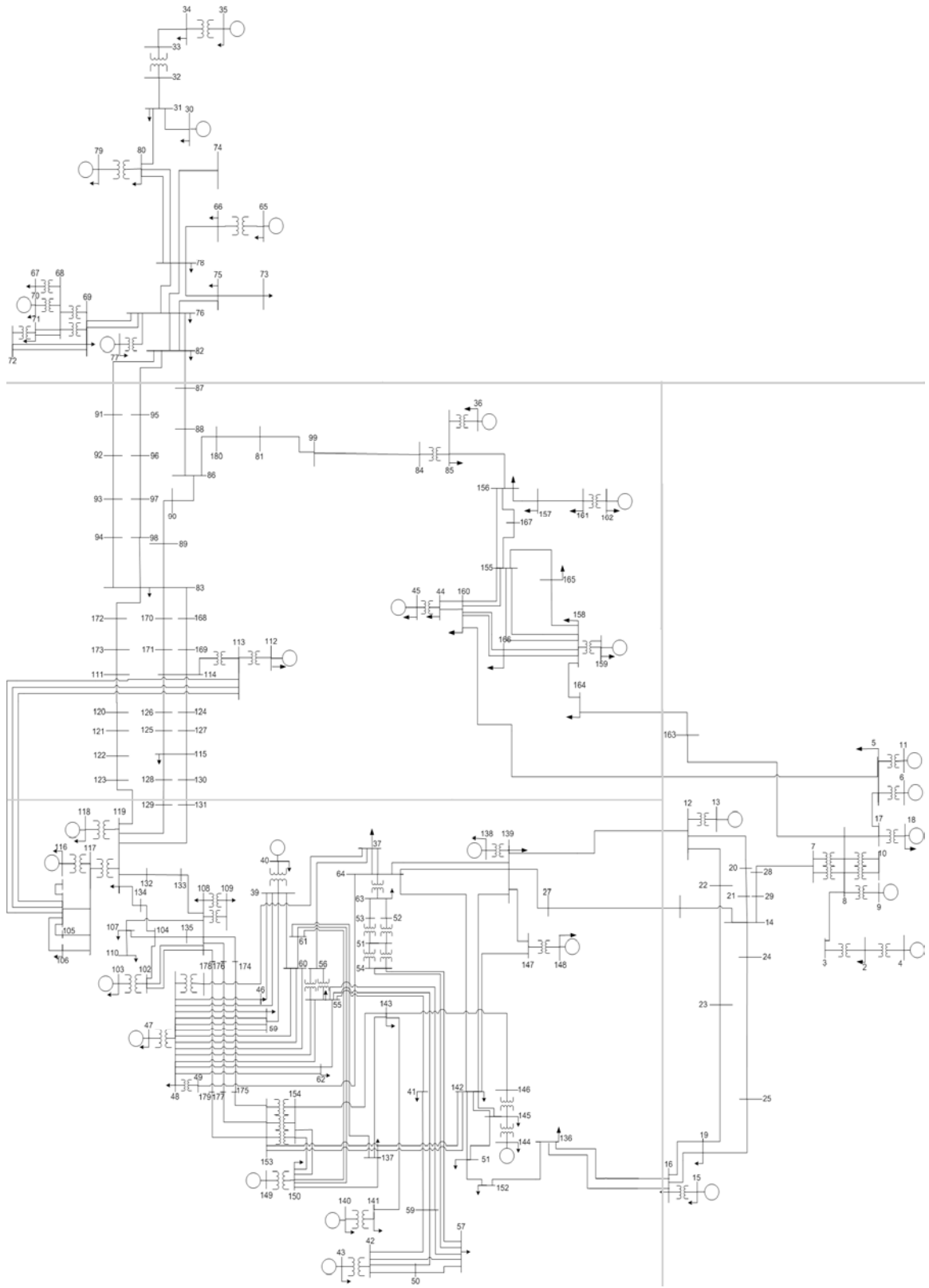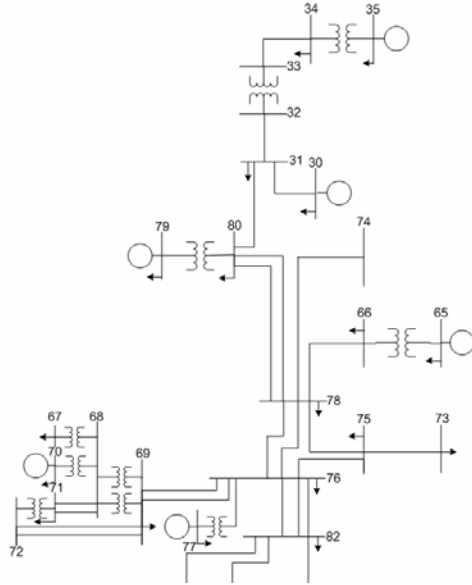
Figure 4.1 WSCC 179-Bus Test System

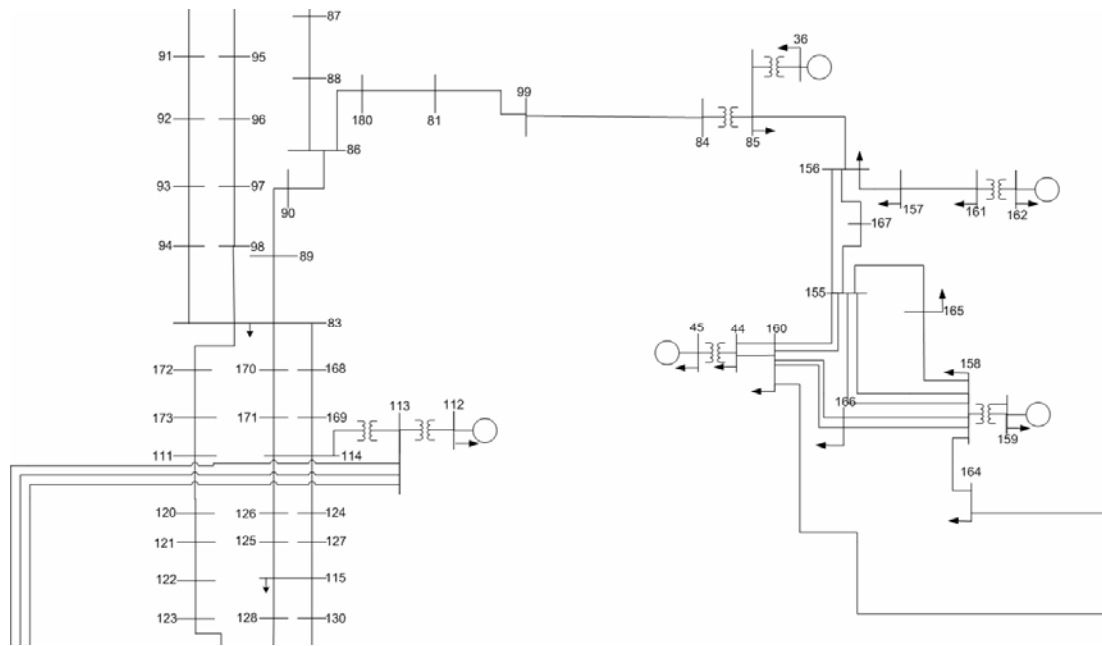Figure 4.2 Top Section of WSCC 179-bus System

Figure 4.3 Middle Section of WSCC 179-bus System
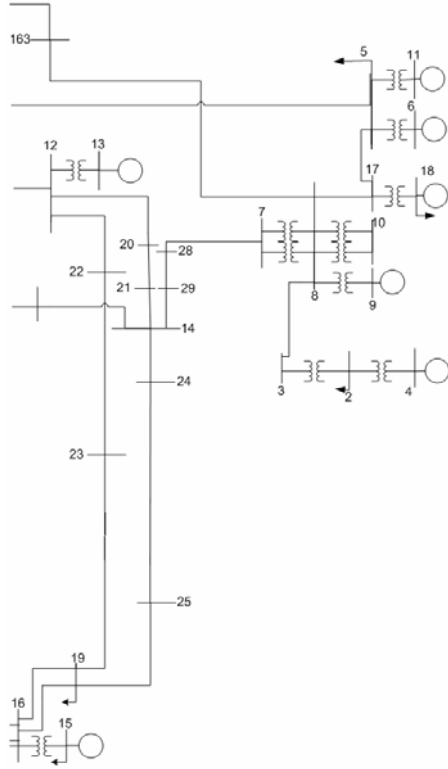
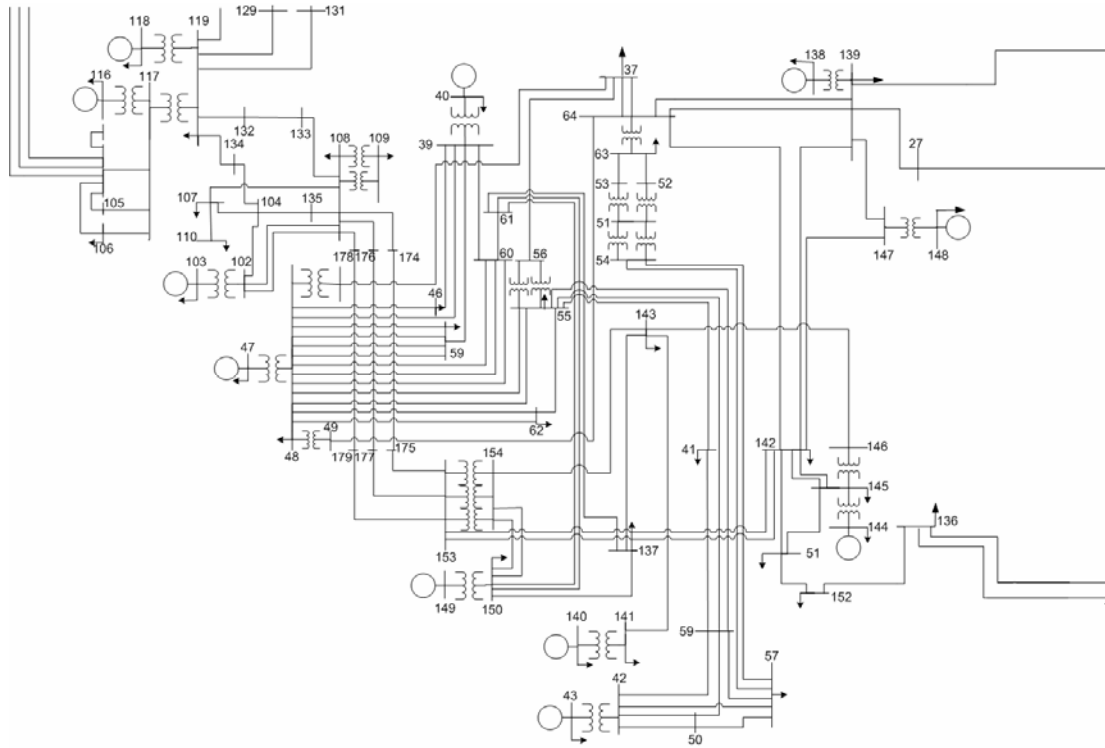Figure 4.4 Right Section of WSCC 179-bus System

Figure 4.5 Bottom Section of WSCC 179-bus System

due to its larger size. When the system is reduced via Kron reduction, effects of

generator current injections still need to be examined at twenty-nine buses. Due to the

overwhelming nature of this problem, a graphical tool was developed that - for a

particular impedance matrix $[\overline{Z}]$ - displays the buses that have large impedance

magnitudes (relative to the other magnitudes in the column) in every column of $[\overline{Z}]$.

These magnitudes correspond to the buses that are most affected by a generator current

injection at a particular bus. As described in Section 3.2, this effect can be correlated to

the amount of influence a particular machine has on another, which can result in two or

more machines being electrically coupled together.

The graphical tool template is a picture approximating the locations of the twenty-

nine machines that are depicted in Figure 4.1. The effects of a current injection from a

generator at a particular bus were represented as a line drawn between that machine and

the machines affected by the current injection. In other words, for a generator at bus i,

lines were drawn between that bus and the buses corresponding to the largest magnitudes

in column i of $[\overline{Z}]$. Because the effect that a current injection from a generator at a

particular bus has on another bus is related to how much influence the machine at the

injected bus has on the machine at the other bus, these lines represent which machines

strongly influence other machines in the power system. Some way to visualize this

influence was needed, so it was determined that the strongest influence would be

represented by a red line, influence of some lesser degree by a yellow line, and even

weaker influence by a green line. Experience with the impedance characteristics of the

179-bus system led to threshold values of 0.00025 per unit, 0.00008 per unit, and 0.00001

per unit to be chosen for the red, yellow, and green lines, respectively. Therefore, the red
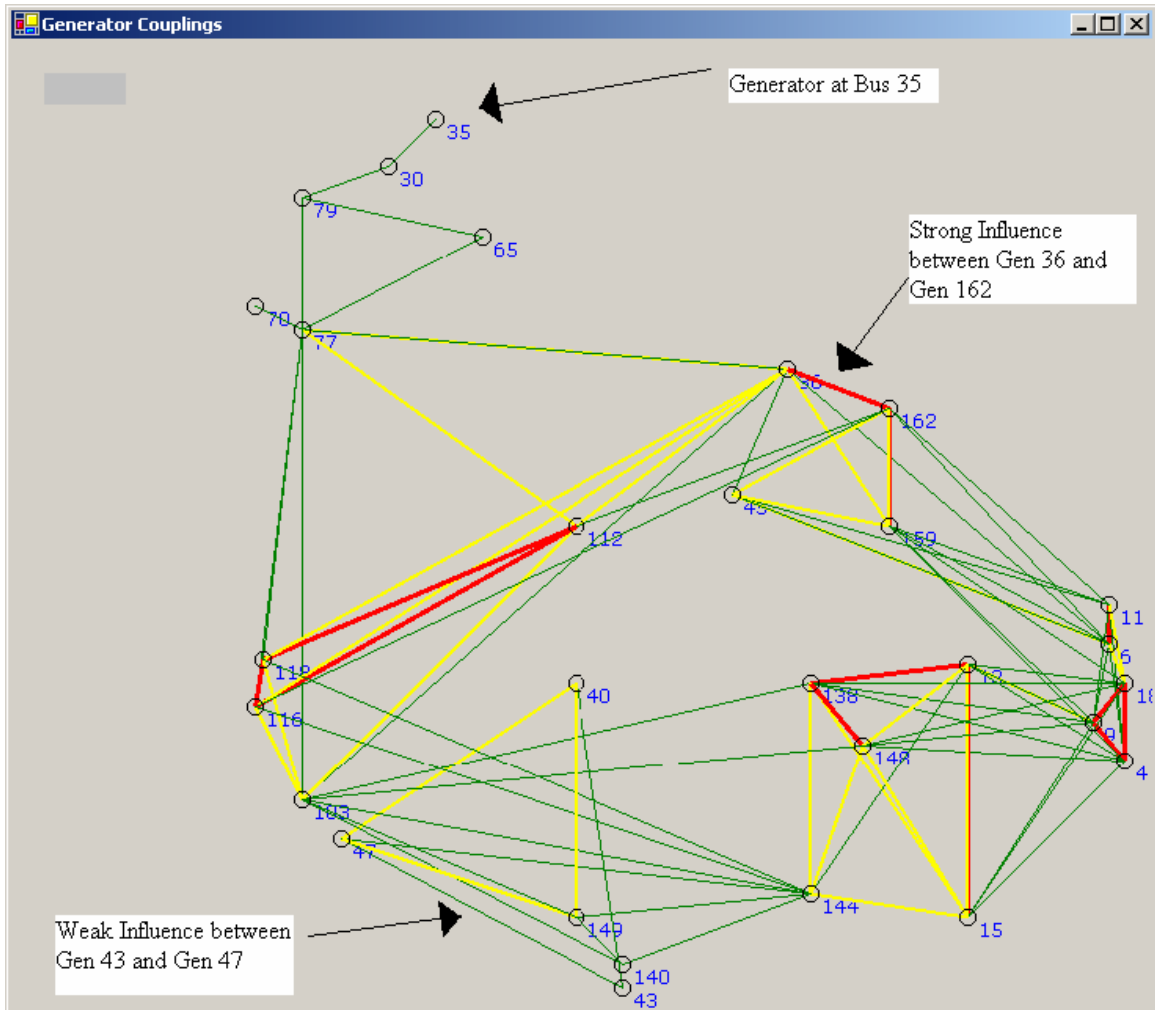
Figure 4.6 Generator Coupling with All Branches in Service

line drawn between generators 36 and 162 in Figure 4.6 means that the magnitude of

$z_{36,162}$ in the 179-bus system impedance matrix is greater than 0.00025 per unit and it

represents a strong influence between generators 36 and 162. These lines are drawn for

all twenty-nine generator buses in Figure 4.6 and are extremely helpful in identifying

groups of machines that influence one another by visually representing the strength of

this influence with red, yellow, and green lines. Accordingly, there appears to be four

areas where generators could be strongly coupled together, as indicated by the groups of

red lines in Figure 4.6.

The situation in Figure 4.6 is one with all branches in service. Notice that changes to the system impedance matrix could result in changes in the colors and directions of the lines in Figure 4.6. For losses of various branches, the Kron-reduced $[\overline{Y}]$ is formed as outlined in the procedure in Chapter 2. The impedance matrix is then formed by inverting $[\overline{Y}]$ and used to get a graphical output similar to Figure 4.6. As with the 5-bus system in Chapter 3, dynamic simulation is needed to verify the results predicted by the graphical tool.

4.3 Contingencies

Several contingencies were placed on the system for purposes of further verifying the generator coupling concepts discussed in Chapter 3. The area of interest in the 179-bus system is the pocket of five generators (4, 6, 9, 11, and 18) that appear to be strongly coupled to one another, according to Figure 4.6. The first contingency to be considered is one close in proximity to this generation pocket, while the second is one further away from the same group of machines.

4.3.1 TL$_{24,25}$

The first contingency used to evaluate the generator coupling concepts is placing a three-phase fault on the transmission line, TL$_{24,25}$, very close to bus 24. Assuming pilot relaying is present and three cycle breakers are used, the bus 24 and bus 25 ends of the faulted line clear in approximately 3 and 4 cycles (50 ms and 66.67 ms for 60 Hz systems), respectively. The graphical depiction of the system machine couplings if TL$_{24,25}$ is taken out of service is shown in Figure 4.7. Notice that generators 4 and 15 were represented as being weakly coupled according to the green line drawn between
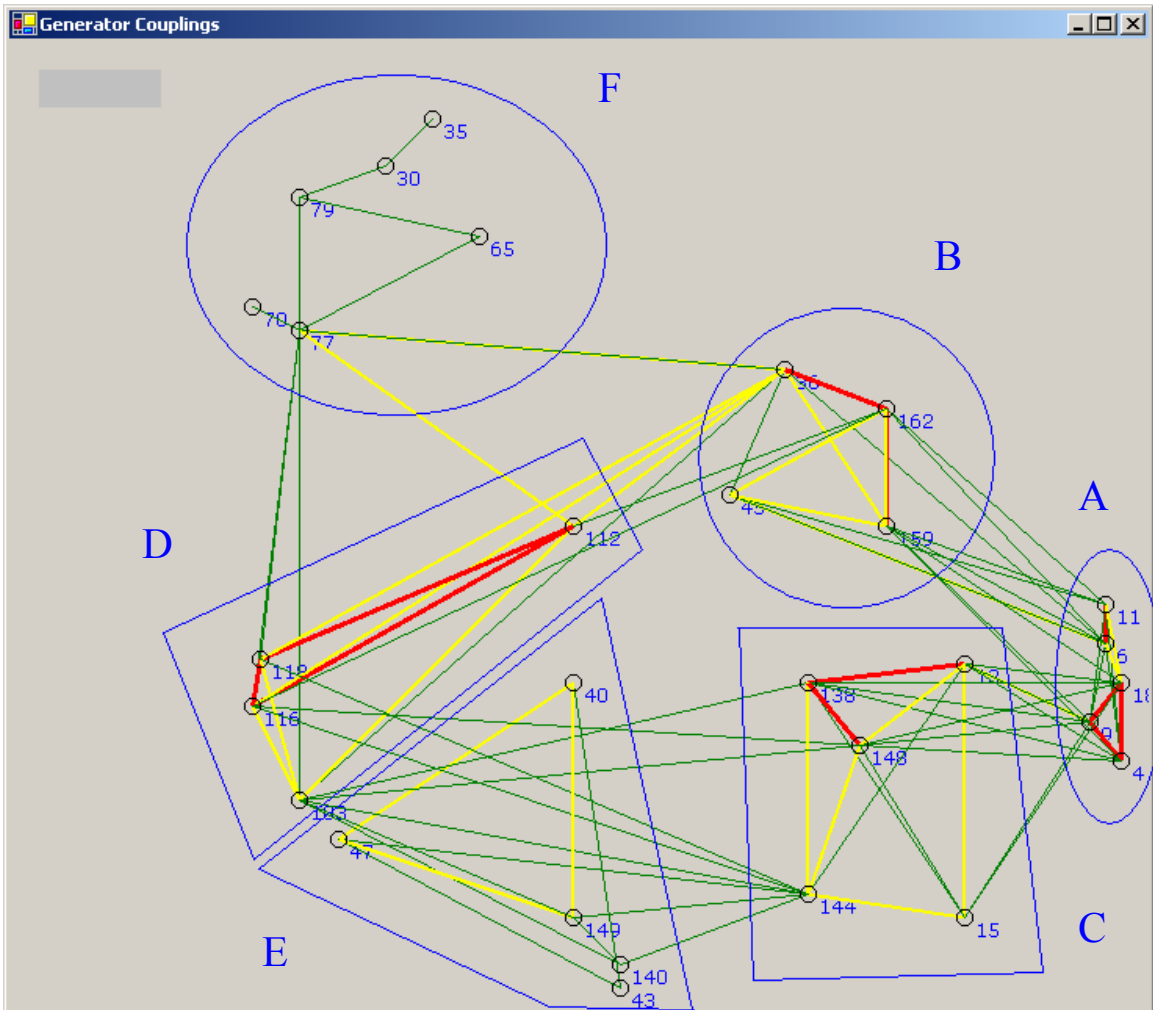
Figure 4.7 Generator Coupling with $TL_{24,25}$ Out of Service

them in Figure 4.6, but upon removal of a piece of the transmission system that links

them ($TL_{24,25}$), they are no longer weakly coupled as indicated by the absence of a

connection between them in Figure 4.7. This appears to be the only major change

between Figures 4.6 and 4.7. Visual inspection is used to separate the machines into six

clusters by only crossing lines that are not red (remembering that a red line indicates the

possibility of two generators being strongly influenced by each other), then crossing

green lines before yellow lines as necessary. These clusters are denoted by the blue lines

that surround the various groups in Figure 4.7 and are listed in tabular form in Table 4.1.

Table 4.1 Generator Clusters in the 179-bus system

Groups	A	B	C	D	E	F
Generators	4	36	13	103	40	65
	6	45	15	112	43	70
	9	159	138	116	47	77
	11	162	140	118	140	79
	18		144		147	30
			148			35

Machine rotor angle plots from the dynamic simulations are shown in Figure 4.8. The fault was placed on $TL_{24,25}$ at t=0 seconds. The plots show the rotor angles from t=0-5 seconds, and they are grouped to correspond to the six clusters seen in Figure 4.7 that were produced by encircling areas while not crossing a red line.

Observation of the rotor angle plots verifies much of what inspection of the graphical depiction of system machine couplings initially revealed. Currently, visual inspection is the method used to compare the rotor angle plots with the results obtained from the impedance matrix. Other means for grouping the rotor angle plots in Figure 4.8 have been attempted but will not work for the general cases presented in this chapter. Descriptions of these methods and reasons for their ineffectiveness are presented in the Appendix.

Cluster A (4, 6, 9, 11, and 18) has rotor angles that move in phase with each other, while also exhibiting similar frequencies. The rotor angles of the machines in cluster B (36, 45, 159, and 162) also move very closely together. The rotor angles of the machines cluster C (13, 15, 138, 144, and 148) move well together except for generator 15. The rotor angles of the machines cluster D (103, 112, 116, and 118) also appears to move well together except for generator 103. In each of the cases mentioned above, there

32
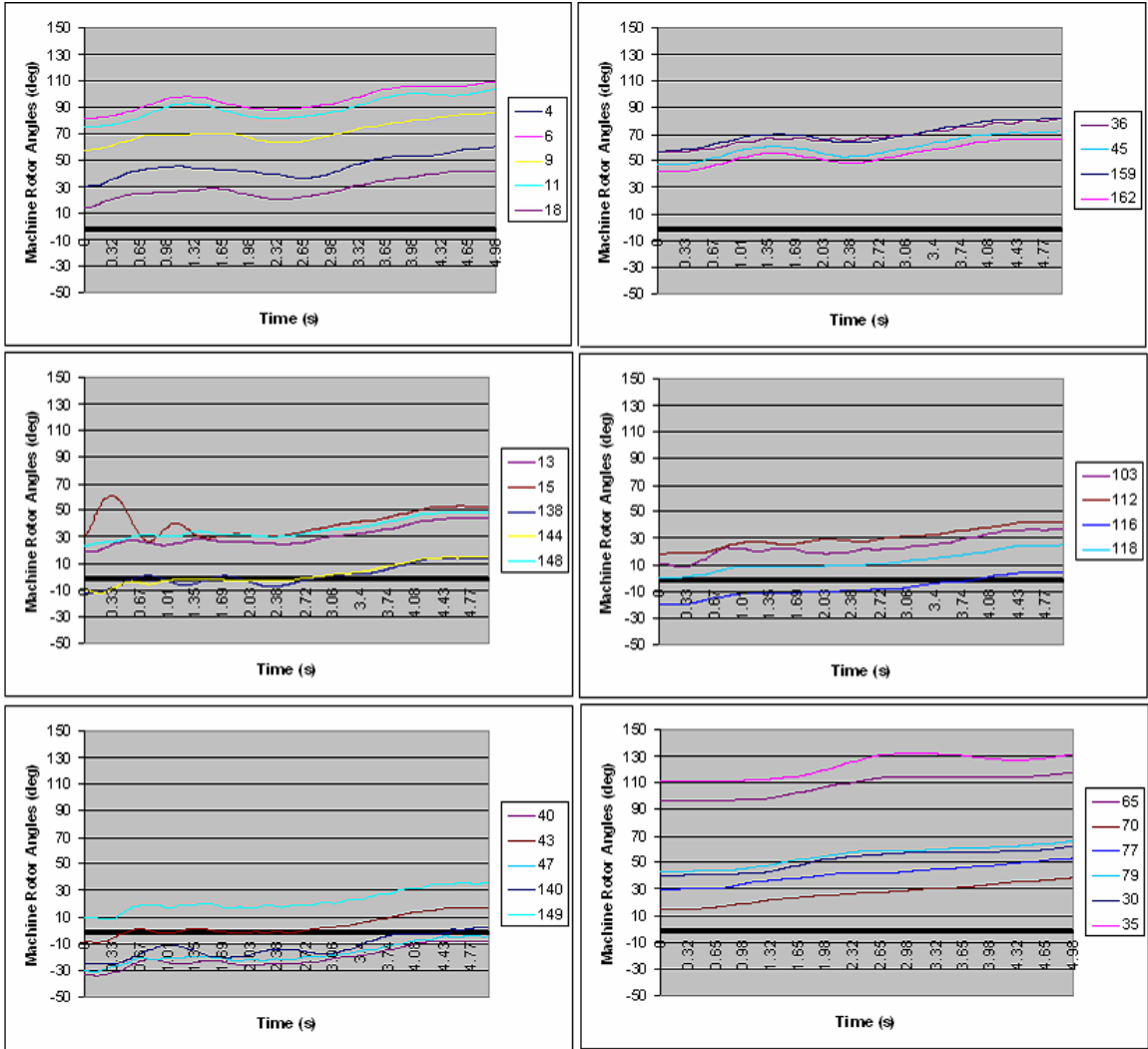
Figure 4.8 Generator Rotor Angles for TL$_{24,25}$ Out of Service

were red lines linking several generators in each group, meaning there were indicators of

possible strong coupling between the generators in each pocket according to the system

impedance data.

Furthermore, the observation that two generators are moving differently than the

rest of their respective groups (15 and 103) could mean they aren't as strongly coupled to

the machines in their group. This observation is in line with the information obtained

from the system impedance matrix shown in Figure 4.7. In both cases, the generators in question (15 and 103) are linked to the others in their groups by yellow lines. These yellow lines represent a weaker coupling than red lines that link the remaining generators in each group. However, another factor that could be causing generator 15 to separate from the rest of the group is the fact that the fault in question is very close in proximity to that specific generator. This, along with the possibility that generator 15 isn't as strongly influenced as the other machines in its group could be cause of its separation as shown in the rotor angle plots.

For the $TL_{24,25}$ contingency, the impedance matrix concepts introduced in Chapter 3 hold up fairly well – especially when considering the generators that are predicted to be strongly coupled to one another as shown in Figure 4.7. As with the 5-bus system, the machine impedances X'_d are not a factor in the generator coupling of the 179-bus system. The WSCC 179-bus system is an equivalent of a much larger power system. Because it is an equivalent system, the 29 generators in the system all have a very large machine base relative to the system power base of 100 MVA. The original X'_d values are in per unit on machine MVA base and they are converted to 100 MVA base for system modeling in $[\overline{Z}]$. Because the machine base is much larger than the system base, the machine impedances are reduced dramatically in the conversion from machine base to system base. Therefore, X'_d is not considered when examining generator influence in the 179-bus system. The next step, however, is to see what happens when the machines on the right side are caused to swing by a fault that is further away in the system.

4.3.2 TL$_{92,93}$

The second contingency used to evaluate the generator coupling concepts is placing a three-phase fault on the transmission line, TL$_{92,93}$. The fault description and subsequent clearing follow the same procedure as the TL$_{24,25}$ fault, with the offending line being taken out of service in approximately four 60 Hz cycles. Again, visual inspection is used to separate the machines into six clusters by the method described in Section 4.3.1. The graphical depiction of the system machine couplings if TL$_{92,93}$ is taken out of service is shown in Figure 4.9.
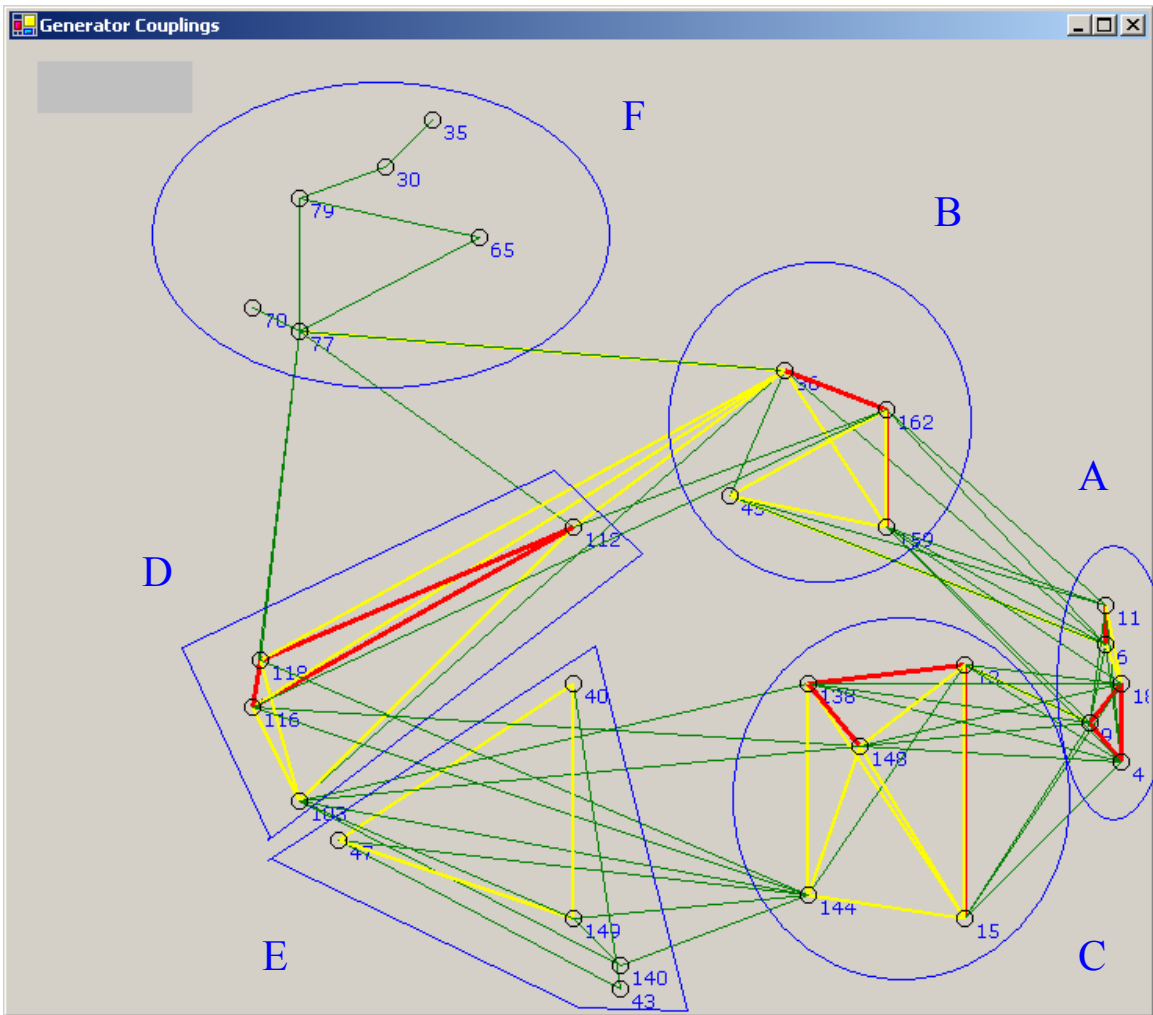

Figure 4.9 Generator Coupling with TL$_{92,93}$ Out of Service

Machine rotor angle plots from the dynamic simulations are shown in Figure 4.10.

The fault was placed on $TL_{92,93}$ at t=0 seconds. The plots show the rotor angles from t=0-

5 seconds, and they are grouped to correspond to the six clusters seen in Figure 4.9 that

were produced by encircling areas as described in Section 4.3.1.

Again, observation of the rotor angle plots verifies much of what inspection of the

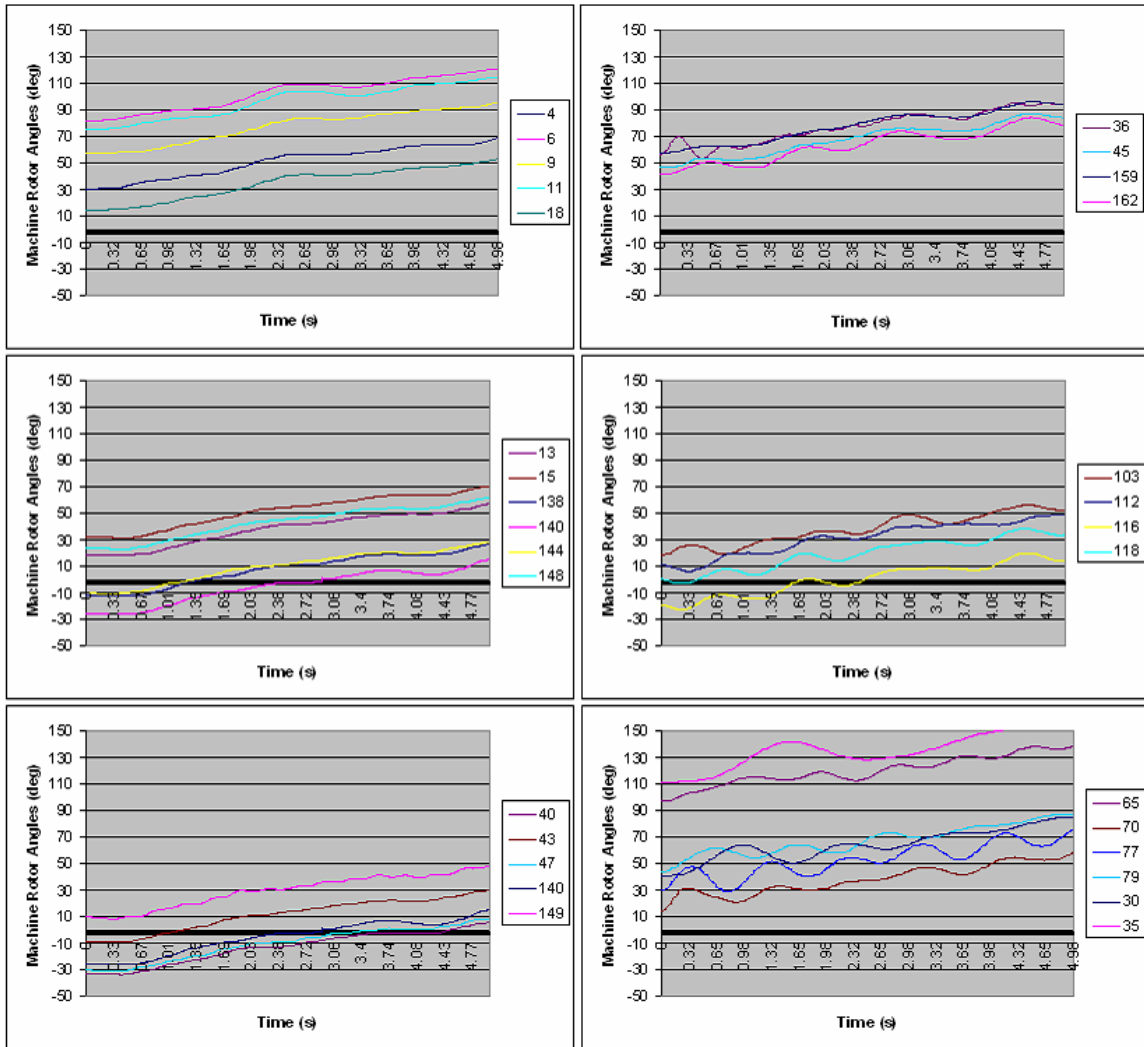graphical depiction of system machine couplings initially revealed. Cluster A (4, 6, 9,

Figure 4.10 Generator Rotor Angles for $TL_{92,93}$ Out of Service

36

11, and 18) still has rotor angles that move in phase with each other, while also exhibiting similar frequencies. The rotor angles of the machines in cluster B (36, 45, 159, and 162) also move very closely together. However, generator 36 appears to have a much more dramatic initial swing than the others in the group. As with the generators in the first contingency, this could be due to the fact that generator 36 is close in proximity to $TL_{92,93}$. Also, observation of Figure 4.9 reveals some intermediate influence (as represented by the yellow lines) between generator 36 and three generators that are quite close to the $TL_{92,93}$ contingency. This influence could also be part of the reason that generator 36 separates from the group designated by visual inspection of Figure 4.9.

The rotor angles of the machines in cluster C (13, 15, 138, 144, and 148) move together better for this contingency than for the contingency at $TL_{24,25}$. This could be due to the fact that generator 15 is no longer strongly influenced by the close proximity of the fault at $TL_{24,25}$. Notice also how generator 15 is strongly coupled to the rest of the group as denoted by the red line between it and generator 13. This was not the case in the $TL_{24,25}$ contingency. Observation of the graphical depiction of the impedance data leads to the conclusion that moving the fault away from generator 15 results in a stronger coupling between it and generator 13 and subsequently the rest of the group.

The rotor angles of the machines in cluster D (103, 112, 116, and 118) also appears to move well together except for generator 103. This was the same result as when $TL_{24,25}$ was taken out of service, which means intermediate influence indicated by the yellow lines extending from generator 103 to the rest of the group could be insufficient to influence the generator to move with the others in the group.

More interesting results are obtained when observing cluster F (30, 35, 65, 70, 77, and 79) of the system. For both contingencies, the green lines are indicative of weak coupling or influence between generators in this group. As demonstrated by observation of the results of the contingency at $TL_{24,25}$ and how the contingency affected machines (13 and 15) that were intermediately influenced by each other, proximity of a fault will have an effect on how well machines move together. When the fault was close to generators 13 and 15, they didn't move very well together in the dynamics. However, when distance was put between the contingency of interest and these two machines, they grouped together quite nicely as seen in Figure 4.10.

A similar situation has taken place for the group of machines in cluster F. For the contingency at $TL_{24,25,}$ they moved together very closely as seen in Figure 4.8. When the fault was moved to $TL_{92,93}$, however, they separated rather dramatically as shown in Figure 4.10. $TL_{92,93}$ is relatively close to this group, but isn't as severe a contingency due to the parallel transmission line adjacent to the line which $TL_{92,93}$ helps comprise. Nonetheless, the group still breaks up as seen in Figure 4.10. This could be due to the weak coupling displayed between generators of the group in Figure 4.9. The fact that they aren't very strongly coupled as a group to begin with could lead to a minor contingency causing them to not move closely with each other.

For the $TL_{92,93}$ contingency, the impedance matrix concepts introduced in Chapter 3 do appear to conservatively help reveal which machines move together, while at the same time showing that proximity of a group of generators to a fault can have an appreciable effect on the group coupling. In terms of the lines drawn in Figures 4.6, 4.7, and 4.9, the red lines represent influence that appears to be immune from fault location,

the green lines represent influence that could be affected by fault location, and the yellow lines represent influence that may or may not be affected by fault location. Overall, observation of results from the 179-bus system reveals that there appears to be reasonable correlation between system impedance and generator coupling.

As previously discussed in Chapter 3, this relationship between system impedance and generator coupling can be used to help determine possible flowgate locations in a power system. Implementing this concept on the larger 179-bus system reveals more interesting results. Observation of Figures 4.6, 4.7, and 4.9 reveals that the system impedance matrix doesn't change very much for the two contingencies considered in this chapter. This means that generator influence doesn't change very much with respect to contingency location, according to the correlation between system impedance and generator influence developed in Chapters 3 and 4. This is especially true for the cases of "strong" influence, as indicated by the red lines in the graphical depictions of the impedance matrix. In particular, groups A, B, and D exhibit the same "strong" influence for both contingencies considered in this chapter.

Having the ability to identify these "strong" influences is quite helpful when considering possible flowgate locations because these groups of coupled machines represent wide-area stability concerns where generation may need to be curtailed. For example, the red lines connecting the machines in group A (4, 6, 9, 11, 18) are indicative of the strong influence exhibited by the machines in group A. Observation of Figure 4.4 reveals the three branches connecting this group of generators to the rest of the system are $TL_{5,160}$, $TL_{8,163}$, and $TL_{7,28}$. The wide-area stability concern involving group A could possibly be lessened if the total flow on these three lines is constrained using a

transmission flowgate. Dynamic simulation could then be used to determine if a flowgate

is actually needed, and if so, what the limiting value of the flowgate should be.

CHAPTER 5

CONCLUSION

The continual increase of generation in localized areas has the potential to threaten a system stability limit due to congested transmission lines. Transmission flowgates are one tool being proposed to help manage this congestion. One problem with flowgates, however, is the absence of a defined procedure used to place one in the system. Developed in this thesis is a method that conservatively identifies potential flowgate locations by determining which generators will swing together due to a contingency in the system. This act of swinging together is denoted as electrical coupling and it is affected by several things, one of which is the system impedance matrix. Detailed in this thesis is the explanation of how system impedances influence the total dynamic coupling. The ability to identify this influence is quite helpful when considering possible flowgate locations because generators that are strongly coupled together will be so without regard to contingency location.

The first step was to build a mathematical model of the power system. The mathematical model obtained was a set of nonlinear coupled differential equations. Once built, the system impedance matrix was extracted from the mathematical model and used to help determine generator coupling by the theory that a 1 per-unit current injection at bus i in the system will result in voltages being produced at all other buses j in the system based on the product $z_{ij} * I_i$. The results produced by this method agreed with the dynamic

results as tested on the 5-bus system. The WSCC 179-bus system was then used to further examine this idea of generator coupling by placing a contingency in various places in the power system relative to a group of electrically coupled generators.

Future work on this method includes abandoning the current method of visual inspection of the dynamic responses of the generators.   Some method should be used to quantify the rotor angle plots so they can be properly compared to the clusters produced by the impedance matrix data. Currently, Prony and fast Fourier transform analyses are being explored as ways to classify the rotor angle plots by phase and frequency. The results of the progress made with these methods are detailed in the appendix. Other future work consists of learning more about how the impedance matrix values can be used as a part of some influence coefficient that can be derived and calculated for a given power system under study. Once derived and calculated, much needs to be learned about how these coefficients can be better utilized to locate flowgates.

REFERENCES

[1]   Valenzuela, Jorge, Halpin, S. Mark, and Park, Chan S., "Generation Expansion Planning in Stability Limited Power Systems," National Science Foundation EPNES Workshop, Puerto Rico, July, 2004.

[2]   Kundur, P., "Power System Stability and Control," McGraw-Hill, New York, 1994.

[3]   Wildi, Theodore, "Electric Machines, Drives, and Power Systems," Prentice Hall, New Jersey, 2002.

[4]   Kamen, Edward, and Heck, Bonnie, "Fundamentals of Signals and Systems using MATLAB," Prentice Hall, New Jersey, 1997.

[5]   Hauer, J.F., "Initial Results in Prony Analysis of Power System Response Signals" IEEE Transactions on Power Systems, Vol. 5, No. 1, Feb., 1994.

APPENDIX

Currently, visual inspection is the only method used to compare the known

behavior of the machines (the machine rotor angle plots) with the estimated behavior of

the machines (the machine influence derived from the system impedance matrix). As

noted in Chapter 5, some preliminary effort has been made to try to numerically quantify

and group the machine rotor angle plots using two methods: fast Fourier transform and

Prony analysis. Neither of these methods has produced reliable results to date. The fast

Fourier transform is unable to produce reliable frequency and phase characteristics due to

exponential decay in the machine rotor angle plots. Prony analysis is unable to produce

reliable results for several reasons, including input data precision and the nonlinear nature

of the power system dynamics. However, the progress made with both methods is

documented for future reference.

7.1 Fast Fourier Transform

The fast Fourier transform, or FFT, takes a discrete signal in the time domain and

transforms that signal into its discrete frequency domain representation [4]. Because all

data points for the machine rotor angle plots are readily available, it is a simple task to

use a signal analysis program (such as MATLAB) to calculate the FFT of each rotor

angle plot. Once calculated, the dominate frequency of the rotor angles could then be

observed from the FFT spectral plots. The machines in the 179-bus system could then be

grouped by their dominate frequency using cluster analysis and compared to the groups observed using the graphical tool in Chapter 4.

An arbitrary exponential function is shown in (7.1) and its corresponding frequency spectrum is shown in Figure 7.1. The frequency spectrum seen in Figure (7.1) is calculated using the FFT.
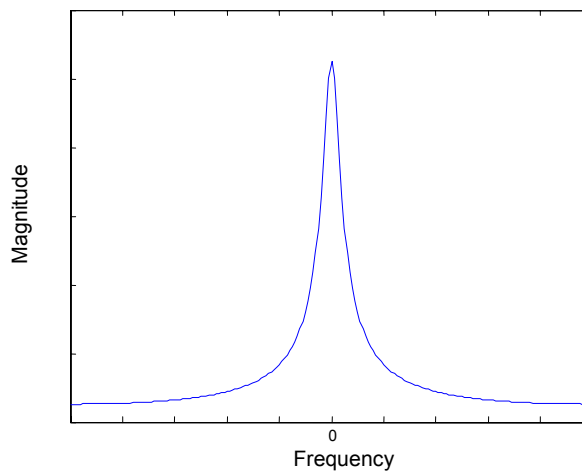
$$y(t) = \exp(-a \cdot t) \tag{7.1}$$

Figure 7.1 Exponential Frequency Spectrum

When the exponential in (7.1) is multiplied by a sine function as in (7.2), the result is an exponentially decaying sine wave of the form in Figure 7.2. The frequency spectrum of this sine wave with exponential decay is shown in Figure 7.3, where ω_1 in (7.2) is given the arbitrary frequency value of ω_0. Observation of Figure 7.3 shows that the sine function shifts the frequency spectrum by the amount of $\pm\,\omega_0$, which is the dominant frequency in (7.2). An additional exponential decay term is added to (7.2) and the result is shown in (7.3).

$$y(t) = \exp\left(\frac{-t}{\tau}\right) \cdot \sin(\omega_1 t) \tag{7.2}$$

45

$$y(t) = \exp\left(\frac{-t}{\tau}\right) \cdot \sin(\omega_1 t) + \exp\left(\frac{-t}{\tau}\right) \cdot \sin(\omega_2 t) \qquad\qquad (7.3)$$
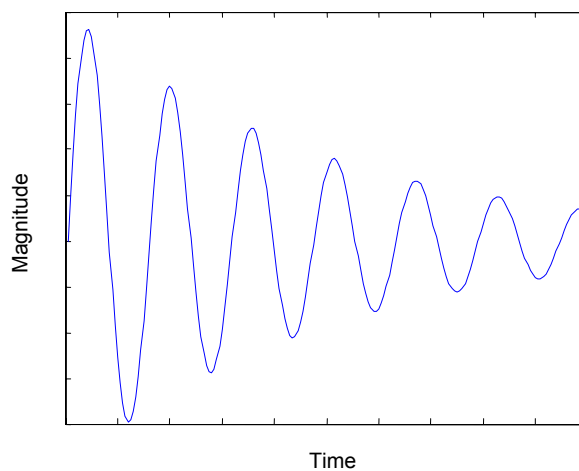

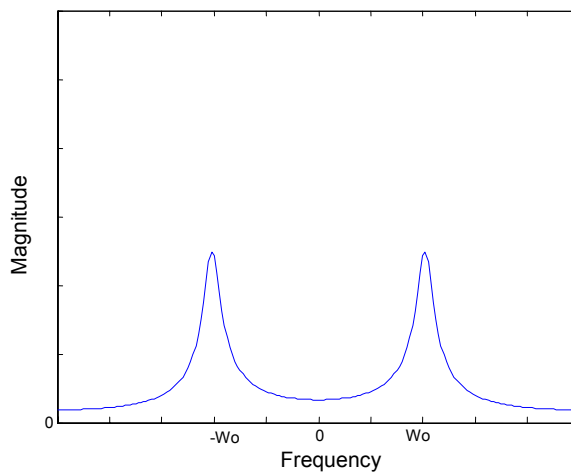Figure 7.2 Time Domain Plot of a Sinusoid with Exponential Decay

Figure 7.3 Frequency Spectrum of a Sinusoid with Exponential Decay

The frequency spectrum shown in Figure 7.4 is plotted from the FFT of (7.3).

The frequency of the additional term ω_2 is twice the value ($\omega_2 = 2\omega_0$) of the original sine

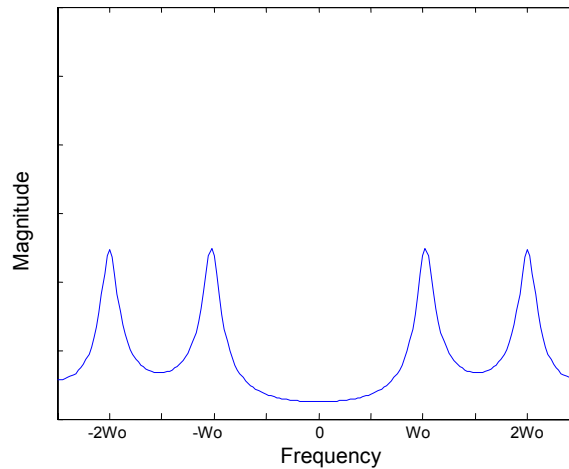function frequency in (7.2).   Notice in Figure 7.4 that in addition to the original "peaks"

Figure 7.4 Frequency Spectrum of Sinusoid with Multiple Exponential Decay Terms

at $\pm\omega_0$ (which represent a high amount of frequency content at $\pm\omega_0$), there are now

peaks at $\pm 2\omega_0$ which are indicative of the second exponential decay term being

introduced in (7.3). The FFT is a very effective tool for distinguishing between the two

dominant frequencies in (7.3).

Complications arise, however, as the frequencies of the exponentially decaying

terms in (7.3) approach the same value. This scenario is depicted in Figure 7.5, where the

frequency of the original sinusoidal term (ω_1) is kept at ω_0, and the second term's

sinusoidal frequency (ω_2) begins at $2\omega_0$ and is systematically reduced so it approaches

ω_0. Observation of Figure 7.5 reveals that as the frequencies of the two terms get closer

and closer together (i.e. as ω_2 approaches ω_0), the spectral plots produced from the FFT

become more and more cluttered. There appears to be one dominant frequency at ω_0 in

the final plot, but in actuality the second decay term is at $1.1\omega_0$. This is very hard to

distinguish in the plot, and is a significant problem when attempting to classify the
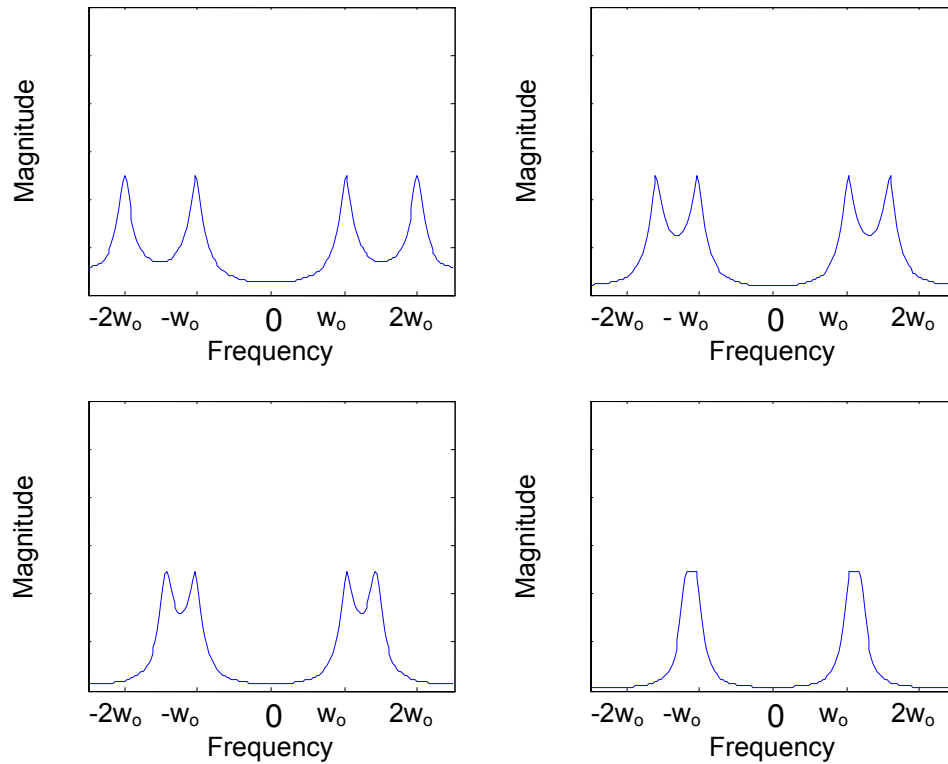
47

Figure 7.5 Frequency Spectra with Muliple Exponential Decay Terms

machine rotor angles of the 179-bus system by frequency and phase using the FFT.

Therefore, when multiple exponential decays are introduced in a signal, the potential is

present for the continuous nature of the exponentials to greatly distort the frequency

spectrum as calculated by FFT to the point where the actual dominant frequency or

frequencies are masked. This is particularly the case when the frequencies of the

multiple exponentially decaying terms are very close in value.

Complications can also arise if the exponentials change in (7.3), because this

affects the rate of decay in frequency. This discussion will remained focused on the

frequencies of the sinusoids, but it should be noted that the multiple exponentials in (7.3) have the potential to present the same problems as the multiple sinusoids.

The time domain response of the rotor angle of generator 6 in the 179-bus test system is plotted in Figure 7.6. The FFT of the same generator rotor angle is shown in Figure 7.7. Notice that, unlike the previous spectrum plots, the continuous nature of the exponential frequency spectrum is not depicted in Figure 7.6. This is the result of window function that is applied to the data before the FFT is calculated. The window function used in the analysis is the rectangular window, which has the frequency spectrum of the well-known "sinc" function. The spectral content of the "sinc" function is what is disrupting the continuous nature of the exponential frequency spectrum. Zero-padding was also implemented when taking the FFT of the machine rotor angle plots. Zero-padding places an equal number of zeros between all terms calculated by the FFT, thus increasing the resolution of the FFT.
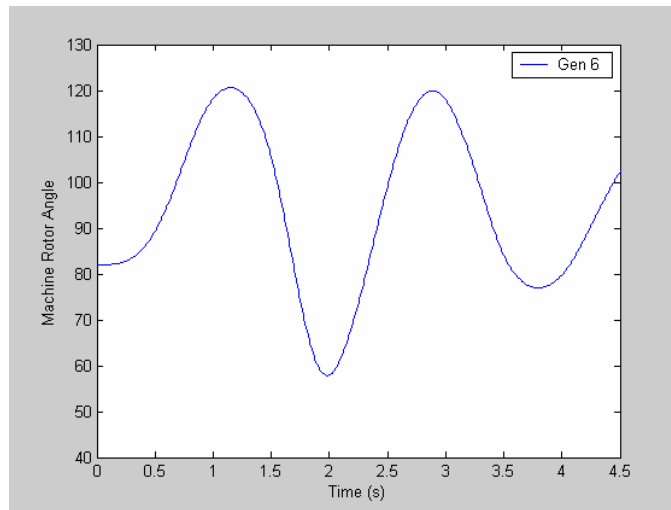

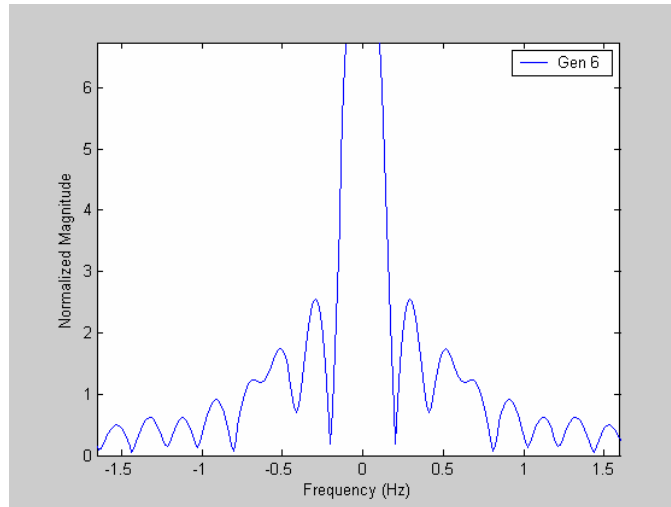Figure 7.6 Time Domain Simulation of Generator 6

Figure 7.7 FFT Results for Generator 6

Observation of the rotor angle plot in Figure 7.6 reveals that the dominant frequency of the signal should be about 0.5 Hz. However, no dominant frequency appears to be present in Figure 7.7. This is the case even though some content is clearly present between 0 and 0.5 Hz as evidenced by the distortion of the sinc function. Similar results were obtained when looking at the spectral content of other machines. In many cases, the only significant spectral content was observed in the dc frequency component, as seen in Figure 7.7. As a result, grouping the machine rotor angles via results obtained by FFT methods does not appear to be generally useful.

7.2 Prony Analysis

Prony analysis extends Fourier analysis by directly estimating the frequency, damping, magnitude, and relative phase of the modal components present in a given signal [5]. This estimation is possible due to the fact that any periodic signal can be represented as a sum of exponentials. Prony analysis uses this fact to curve fit an observed signal y(t) to the expression in (7.4).

$$\hat{y}(t) = \sum_{i=1}^{n} A_i \exp(\sigma_i t)\cos(2\pi f_i t + \phi_i) \tag{7.4}$$

The terms in (7.4) can be rewritten as shown in (7.5), where λ_i represents the modes of the estimated signal $\hat{y}(t)$.

$$\hat{y}(t) = \sum_{i=1}^{n} B_i \exp(\lambda_i t) \tag{7.5}$$

The signal $y(t)$ is sampled N times and in this derivation N is chosen to be twice the number of modes, or N=2n. These samples are evenly spaced by an amount Δt. At the sample times t_k (where k=0, 1, ... , N-1) the exponential in (7.5) is rewritten as shown in (7.6), which produces (7.7). The terms in (7.7) are expanded as shown in (7.8).

$$z_i^{\,k} = \exp(\lambda_i k \Delta t) \tag{7.6}$$

$$\hat{y}(k) = \sum_{i=1}^{P} B_i z_i^{\,k} \tag{7.7}$$

$$\begin{bmatrix} z_1^{\,0} & z_2^{\,0} & \cdots & z_n^{\,0} \\ z_1^{\,1} & z_2^{\,1} & \cdots & z_n^{\,1} \\ \vdots & \vdots & \ddots & \vdots \\ z_1^{\,N-1} & z_2^{\,N-1} & \cdots & z_n^{\,N-1} \end{bmatrix} \begin{bmatrix} B_1 \\ B_2 \\ \vdots \\ B_{n-1} \end{bmatrix} = \begin{bmatrix} y(0) \\ y(1) \\ \vdots \\ y(N-1) \end{bmatrix} \tag{7.8}$$

The vector $\tilde{B}$ is the collection of complex magnitudes that partly comprise (7.5). The rest of (7.5) is comprised of the values in the matrix [Z] and are the complex modal frequencies for the signal. Notice that because $\exp(\lambda_i \Delta t)$ is raised to some power, as indicated by the term $z_i^{\,k}$, the exponents add. So, $z_i^{\,k}$ is equivalent to $\exp(\lambda_i k \Delta t)$ and $(k \Delta t)$ is equivalent to time progressing as k increases. Also notice that [Z] is not the impedance matrix discussed earlier. It is simply a matrix of coefficients used to represent $\exp(\lambda_i k \Delta t)$. If the matrix [Z] and vector $\tilde{B}$ can be solved for then a $\hat{y}(k)$ can be found

that is equal to y(k) (assuming the signal is noise-free). To solve for [Z] and $\widetilde{B}$, the roots

of the nth-order polynomial in (7.9) are calculated, where the terms a_i are unknown

coefficients.

$$z^n - (a_1 z^{n-1} + a_2 z^{n-2} + \cdots + a_n z^0) = 0 \qquad (7.9)$$

The nth-order polynomial in (7.9) can be written because of the assumption that

$y(t)$ is the output of some linear nth-order system. This means that there are n

eigenvalues that can be found from the roots of the characteristic equation of the system.

Observation of (7.6) reveals that the z_i terms in (7.8) are associated with the system

eigenvalues due to z_i simply being shortcut notation for $\exp(\lambda_i \Delta t)$. Because of this, each

z_i in (7.8) is a root of the nth-order polynomial in (7.9). Finding the unknown

coefficients a_i in (7.9) enables the roots of the polynomial and the modes of the response

signal to be calculated.

A (1xN) vector of the unknown a_i coefficients in (7.9) is formed in (7.10) and

multiplied to both sides of (7.8). The right side of the resulting equation is seen in (7.11)

and the left side is (7.12), which is expanded to the form shown in (7.13).

$$\widetilde{A} = \begin{bmatrix} -a_n & -a_{n-1} & \cdots & -a_1 & 1 & 0 & \cdots & 0 \end{bmatrix} \qquad (7.10)$$

$$\widetilde{A}\widetilde{Y} = y(n) - \left[a_1 y(n-1) + \cdots + a_n y(0) \right] \qquad (7.11)$$

$$\widetilde{A}\widetilde{Y} = \widetilde{A}[Z]\widetilde{B} \qquad (7.12)$$

$$\widetilde{A}\widetilde{Y} = B_1 \left[z_1^n - \left(a_1 z_1^{n-1} + a_2 z_1^{n-2} + \cdots + a_n z_1^0 \right) \right]$$

$$+ B_2 \left[z_2^n - \left(a_1 z_2^{n-1} + a_2 z_2^{n-2} + \cdots + a_n z_2^0 \right) \right] + \dots = 0 \qquad (7.13)$$

52

The summation of terms in (7.13) that is multiplied by B_1 is equal to zero because z_1 in (7.13) is a root of the characteristic equation in (7.9). Additionally, summation of terms in (7.13) that is multiplied by B_2 is equal to zero because z_2 in (7.13) is a root of the characteristic equation in (7.9). The equation in (7.14) can be formed from (7.11) due to the fact that $\widetilde{A}\widetilde{Y} = 0$ as shown in (7.13).

$$-a_n y(0) - a_{n-1} y(1) - \cdots - a_1 y(n-1) + y(n) = 0 \tag{7.14}$$

Observation of (7.12) reveals that the entries in $\widetilde{A}$ can be arbitrarily placed because $\widetilde{A}$ is multiplied by both sides of the equation in (7.12). Because $y(0)\ldots y(n)$ are known, (7.14) is one equation in n unknowns. Additional equations are necessary to determine the coefficients a_i. One approach is to shift the non-zero entries in (7.12) right by one column (and subsequently inserting a zero into the first column) in $\widetilde{A}$ effectively samples the data one increment later. This shift results in the new (1xN) vector shown in (7.15). The vector in (7.15) is applied to (7.8) to get (7.16). As before, the right side of the resulting equation is seen in (7.16) and the left side is (7.17), which is expanded to the form shown in (7.18). Note that the terms in (7.18) are still equal to zero because all terms in (7.18) are simply the terms in (7.13) multiplied by a factor equal to z_i^1.

$$\widetilde{A} = \begin{bmatrix} 0 & -a_n & -a_{n-1} & \cdots & -a_1 & 1 & 0 & \cdots & 0 \end{bmatrix} \tag{7.15}$$

$$\widetilde{A}\widetilde{Y} = y(n+1) - \left[a_1 y(n) + \cdots + a_n y(1) \right] \tag{7.16}$$

$$\widetilde{A}\widetilde{Y} = \widetilde{A}[Z]\widetilde{B} \tag{7.17}$$

$$\hat{A}\widetilde{Y} = B_1 \left[z_1^{n+1} - \left(a_1 z_1^n + a_2 z_1^{n-1} + \cdots + a_n z_1^1 \right) \right]$$

$$+ B_2 \left[z_2^{n+1} - \left(a_1 z_2^n + a_2 z_2^{n-1} + \cdots + a_n z_2^1 \right) \right] + \ldots = 0 \tag{7.18}$$

As seen before in the formulation of (7.14), (7.19) can be formed due to the fact that $\widetilde{A}\widetilde{Y} = 0$.

$$-a_n y(1) - a_{n-1} y(2) - \cdots - a_1 y(n) + y(n+1) = 0 \qquad (7.19)$$

The two equations (7.14) and (7.19) have been derived to help determine the n unknowns a_i. The steps in (7.10)-(7.19) can be applied repeatedly to form all equations that comprise (7.20), which can be solved for the coefficients a_i that were unknown in (7.9).

$$\begin{bmatrix} y(n-1) & y(n-2) & \cdots & y(0) \\ y(n) & y(n-1) & \cdots & y(1) \\ y(n+1) & y(n) & \cdots & y(2) \\ \vdots & \vdots & \ddots & \vdots \\ y(N-2) & y(N-3) & \cdots & y(N-n-1) \end{bmatrix} \begin{bmatrix} a_1 \\ a_2 \\ a_3 \\ \vdots \\ a_n \end{bmatrix} = \begin{bmatrix} y(n) \\ y(n+1) \\ y(n+2) \\ \vdots \\ y(N-1) \end{bmatrix} \qquad (7.20)$$

The solution of (7.20) enables the coefficients of the nth-order polynomial in (7.9) to be specified and rooted to find the z_i coefficients in the first row (k=0) of [Z]. The additional rows in [Z] can be calculated by simply taking each entry in the first row to the kth power (which corresponds to the kth row in [Z]). Once [Z] is calculated, the vector $\widetilde{B}$ can be calculated and solved for in (7.8).

Knowing $\widetilde{B}$ and [Z], the estimated curve fit $\hat{y}(k)$ of the original signal y(t) can be obtained. Once a curve fit is obtained, the frequency and phase of the dominant term of the exponential fit (the dominant mode) can be calculated. As with the FFT method, the machines in the 179-bus system could then be grouped by their dominate phase and frequency using cluster analysis and compared to the groups observed using the graphical tool in Chapter 4.

The curve fit and original plot of two machines in the 179-bus system (generators 6 and 11) are shown in Figure 7.8. Observation of Figure 7.8 reveals that these two

generators have very similar phase and frequency characteristics. Therefore, the

dominant terms of the curve-fit of the two rotor angle plots should also have similar

characteristics. The dominant terms and their corresponding magnitudes, exponential

decay, frequency, and phase are seen in the top half of Table 7.1. As an example of the

form of the resulting estimated equations, the calculated coefficients that correspond to

the dominant eigenvalue of generator 6 in Table 7.1 are substituted into (7.5) and the

result is shown in (7.15). Note that only one term is shown in (7.15). The actual curve fit

is comprised of multiple terms of the form of (7.15) that sum to produce the curve fit seen

in Figure 7.8. The positive exponential decay displayed in Table 7.1 and seen again in

(7.15) is a concern and is discussed later in this section.

$$\hat{y}(t) = 4.2037 \exp(.20661 \cdot t)\cos(2\pi \cdot .42374 \cdot t - 109.86°) \qquad (7.15)$$

Observation of Table 7.1 reveals that the dominant exponential terms of the

curve-fit calculated by Prony analysis share similar magnitudes, exponential decay,

frequency and phase. This is the expected result due to the fact that visual inspection of

the rotor angle plots concludes that they are indeed similar waveforms because of their in

phase behavior. Therefore, Prony analysis has the capability of accurately curve fitting

the machine rotor angle plots.

Unfortunately, similar results were not obtained when all twenty-nine rotor angle

plots from the 179-bus system were curve fit with Prony analysis. The curve fit and

original plot of two different machines (generators 4 and 18) are shown in Figure 7.9. As

in Figure 7.8, these two machines again have very similar phase and frequency

characteristics. However, observation reveals that the curve fit is not as accurate as it

was for the first set of generators - especially after 2.5 seconds into the simulation. Still,

55

Table 7.1 Prony Analysis Results for Various Generators

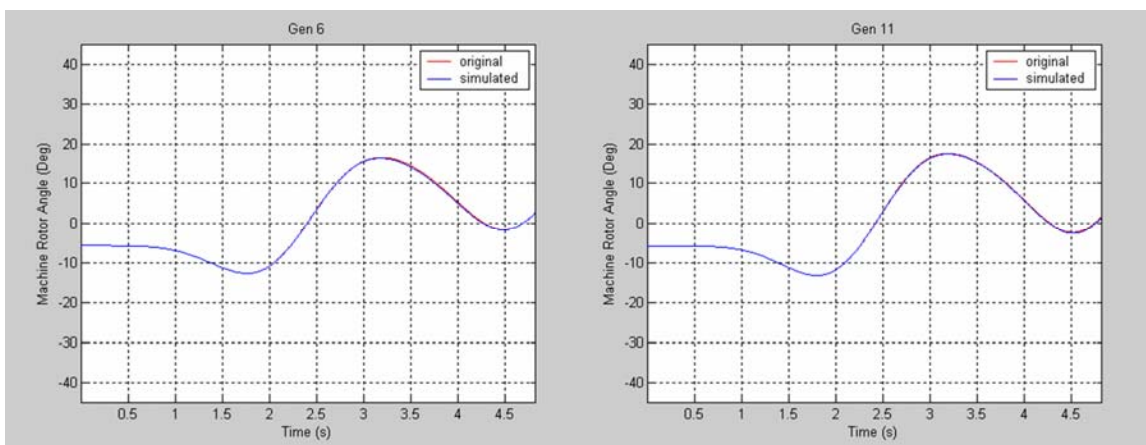| Generator	Dominant Curve Characteristics			
	Magnitude	**Exp Decay**	**Frequency (Hz)**	**Phase (Deg)**
6	4.2037	0.20661	0.42374	-109.85797
11	4.43115	0.21257	0.42325	-110.65684
4	17.48716	-0.29689	0.19715	106.77783
18	39.34433	-0.6588	0.26692	63.14528

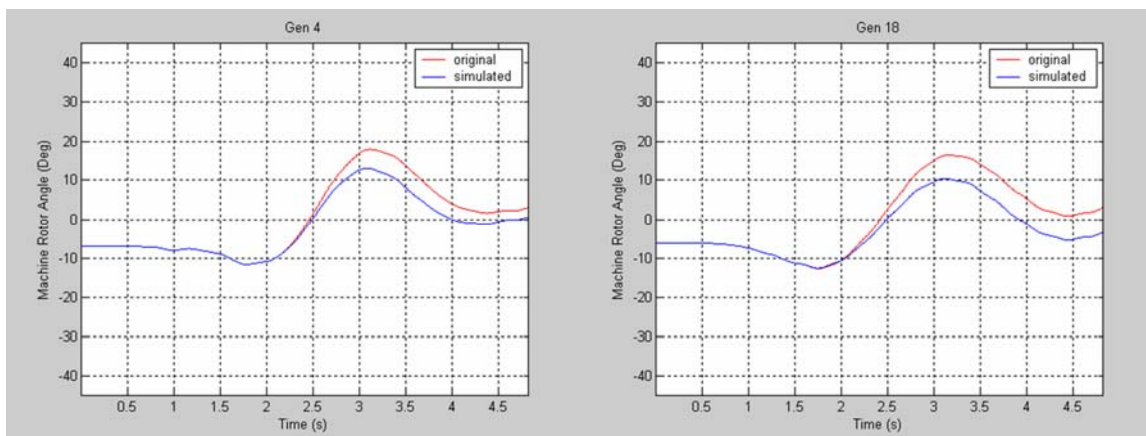Figure 7.8 Prony Analysis Results for Generators 6 and 11

Figure 7.9 Prony Analysis Results for Generators 4 and 18

even with this inaccuracy, the curve fits appear to be quite similar to each other and should exhibit similar characteristics.

The characteristics of the Prony analysis curve fit of the machine rotor angles are seen in the bottom half of Table 7.1. The results are not as favorable as they were for generators 6 and 11. Even though the curve fits for the two rotor angles appear to be quite similar in Figure 7.9, the results seen in the dominant terms calculated using Prony analysis do not exhibit similar characteristics. For example, the two waveforms appear to be in phase with one another in Figure 7.9, but the dominant terms of the curve fit are more than 40 degrees out of phase with one another. This large disparity in the phase of the dominant terms leads to these two generators being placed into separate groups when a k-type clustering algorithm is used to sort the generators into groups according to the information gathered from the Prony analysis curve fit. This should not be the case according to their actual time-domain response seen in Figure 7.9. Also, the positive exponential decay calculated and shown for generators 6 and 11 in the top half of Table 7.1 is another indication that somehow the Prony analysis isn't working in this specific case.

The inaccuracies of the Prony analysis can possibly be attributed to several different issues. One issue is the precision of the data used to plot the machine rotor angles. The simulation tool used to generate the plots, PSSPLT, only outputs the data to 10^{-4} precision. This lack of precision has the potential to compound when using a large number of modal terms to estimate a particular curve.

Also, the fact that Prony analysis is associated with eigenvalues means adopting a linear assumption set for the system response. Power system dynamics are not linear for

large disturbances [2], so the responses seen in rotor angle plots don't have any guarantee of fitting the linear eigen-based analysis assumptions. The disturbances used when analyzing the WSCC 179-bus system were balanced three-phase faults left on the system for a relatively lengthy amount of time, therefore attempting to apply Prony analysis when fitting the rotor angle plots for the large disturbances could be another reason for the inaccuracies seen in Figure 7.9.

While many characteristics of many generators in the 179-bus system are accurately estimated using Prony analysis, there are several others that exhibit problems similar to the ones seen by generators 4 and 18. These inaccuracies result in clusters that do not accurately depict the groups of generators seen in Figures 7.8 and 7.9. Until an accurate method of numerically describing the plots in Figures 7.8 and 7.9 is obtained, visual inspection appears to be the best way to separate the machine rotor angle plots into their respective groups.